iScience

CellPress
OPEN ACCESS

Article

# Cytokeratin 5 determines maturation of the mammary myoepithelium

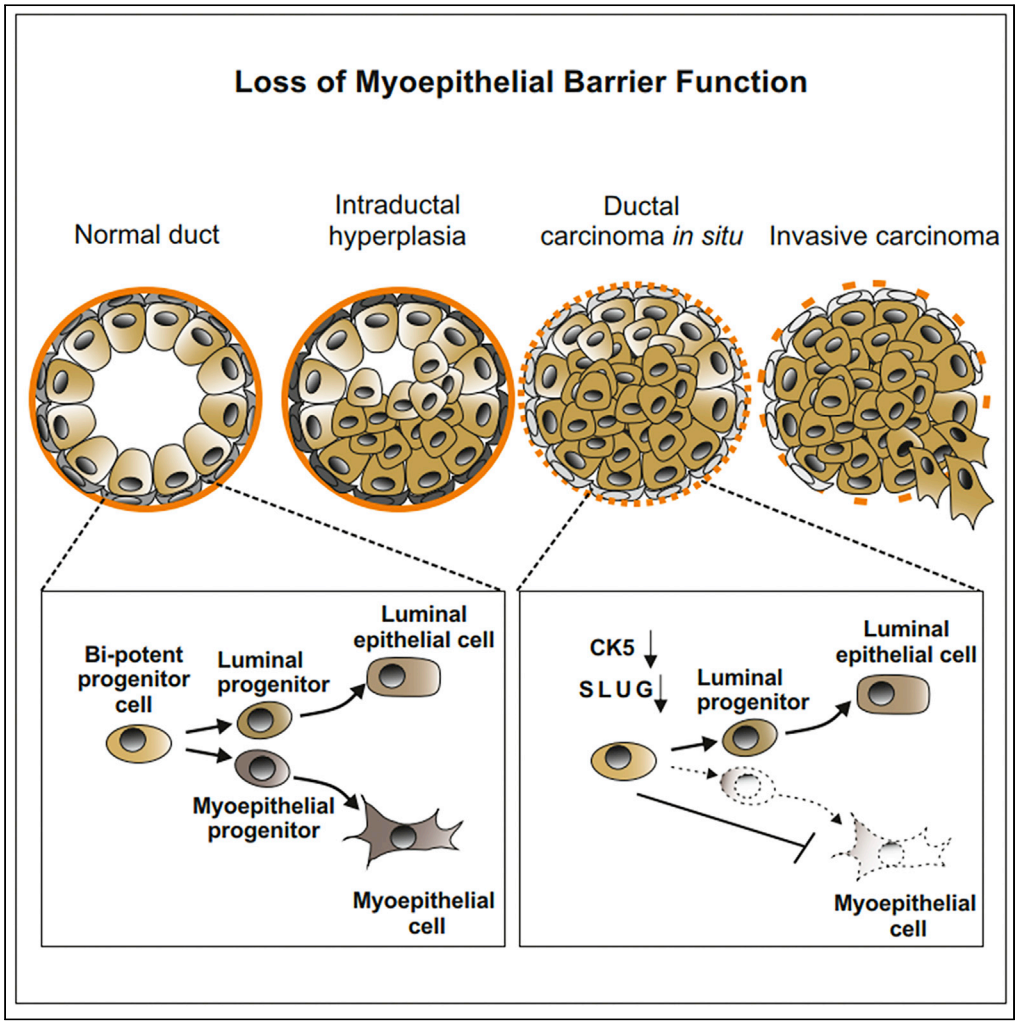


Vivi Deckwirth, Eeva Kaisa Rajakylä, Sandhanakrishnan Cattavarayane, ..., Pia Björkenheim, Antti Sukura, Sari Tojkander

sari.tojkander@helsinki.fi

## Highlights

Cytokeratin 5 (CK5) impacts mammary epithelial cell lineage differentiation

CK5 loss at pre-invasive stage causes impaired maturation of myoepithelial cells

CK5 loss causes SLUG downregulation and differentiation bias in mammary progenitors

Deckwirth et al., iScience *24*, 102413
May 21, 2021 
https://doi.org/10.1016/j.isci.2021.102413

iScience

CellPress
OPEN ACCESS

Article

# Cytokeratin 5 determines maturation of the mammary myoepithelium

Vivi Deckwirth,[1,5] Eeva Kaisa Rajakylä,[1,5] Sandhanakrishnan Cattavarayane,[1] Anna Acheva,[1] Niccole Schaible,[2] Ramaswamy Krishnan,[2] Juan José Valle-Delgado,[3] Monika Österberg,[3] Pia Björkenheim,[4] Antti Sukura,[1] and Sari Tojkander[1,6,*]

## SUMMARY

**At invasion, transformed mammary epithelial cells expand into the stroma through a disrupted myoepithelial (ME) cell layer and basement membrane (BM). The intact ME cell layer has thus been suggested to act as a barrier against invasion. Here, we investigate the mechanisms behind the disruption of ME cell layer. We show that the expression of basal/ME proteins CK5, CK14, and α-SMA altered along increasing grade of malignancy, and their loss affected the maintenance of organotypic 3D mammary architecture. Furthermore, our data suggests that loss of CK5 prior to invasive stage causes decreased levels of Zinc finger protein SNAI2 (SLUG), a key regulator of the mammary epithelial cell lineage determination. Consequently, a differentiation bias toward luminal epithelial cell type was detected with loss of mature, α-SMA-expressing ME cells and reduced deposition of basement membrane protein laminin-5. Therefore, our data discloses the central role of CK5 in mammary epithelial differentiation and maintenance of normal ME layer.**

## INTRODUCTION

Mammary gland parenchyme forms a ducto-lobular tree with a bilayered epithelium. The inner layer of luminal epithelial (LE) cells is surrounded by a basal/myoepithelial layer, which comprises contractile myoepithelial (ME) cells, mammary stem cells, and epithelial progenitor cells, delimited by the basement membrane (BM) from the connective tissue stroma. The basal cell layer is able to regenerate the whole mammary gland epithelial tree (Böcker et al., 2002; Boecker and Buerger, 2003; Van Keymeulen et al., 2011). Development of LE and ME cells occurs in a complex hierarchical manner from the basal progenitors that can differentiate into both epithelial cell types depending on numerous signaling pathways and hormonal stimuli (Arendt and Kuperwasser, 2015; Böcker et al., 2002; Boecker and Buerger, 2003; Boecker et al., 2018; Van Keymeulen et al., 2011). This epithelial differentiation process can be followed as changes in cell-type specific protein expression patterns, including expression of distinct cytokeratin (CK) family members (Böcker et al., 2002; Boecker and Buerger, 2003; Boecker et al., 2018). Less than 5% of the mammary basal cells represent mammary stem cells that express CK5 without luminal epithelial (LE) markers CK8/18/19 or myoepithelial (ME) marker α-SMA (Böcker et al., 2002; Fu et al., 2020). Expression of CK5 is also detected in the progenitor cells that can differentiate into mature luminal or ME cells, lacking the expression of CK5 (Böcker et al., 2002; Boecker and Buerger, 2003; Boecker et al., 2018). Additionally, progenitor cell activity has been attributed to cells expressing CK14 simultaneous with LE or ME markers (Arendt et al., 2014; Boecker et al., 2018; Fridriksdottir et al., 2017; Villadsen et al., 2007). While CKs are filament-forming proteins that mechanically support the cell structure, they have also been attributed to other regulatory functions, such as coordination of nuclear morphology, cell proliferation and apoptosis (Bozza et al., 2018; Iyer et al., 2013; Pan et al., 2013; Weng et al., 2012). Whether basal CK5 has other than structural roles in mammary stem and progenitor cells has not been assessed.

Stem or progenitor cells have been suggested to act as targets for neoplasia initiating transformation (Jiang et al., 2010; Molyneux et al., 2010; Reya et al., 2001). Most mammary carcinomas represent malignant intraductal hyperplasia of epithelial cell origin. Non-invasive and invasive intraductal proliferative lesions are distinguished. Non-invasive lesions comprise usual ductal hyperplasia (UDH), atypical ductal hyperplasia (ADH) and ductal carcinoma *in situ* (DCIS) (Schnitt et al., 2012). Long-term follow-up studies have shown

[1]Section of Pathology, Department of Veterinary Biosciences, University of Helsinki, Agnes Sjöberginkatu 2, Helsinki 00014, Finland

[2]Beth Israel Deaconess Medical Center, Harvard Medical School, Boston, MA 02215, USA

[3]Department of Bioproducts and Biosystems, School of Chemical Engineering, Aalto University, Espoo 00076, Finland

[4]Veterinary Teaching Hospital, University of Helsinki, Helsinki 00014, Finland

[5]These authors contributed equally

[6]Lead contact

*Correspondence: sari.tojkander@helsinki.fi

https://doi.org/10.1016/j.isci.2021.102413

that in time DCIS cases without treatment may develop into invasive carcinomas and may eventually lead to distant metastasis. The percentage of transformed cases varies amongst others according to follow-up time and grade of lesion, with values for low-grade ranging between 18 and 50%, for intermediate grade between 32 and 33% and for high-grade between 17.6 and 67%, respectively (Collins et al., 2005; Maxwell et al., 2018; Ryser et al., 2019; Sanders et al., 2005, 2015). The invasive stage is determined when the boundary provided by ME cells and BM is disrupted. Therefore the ME cell layer has been suggested to act as a barrier against invasion.

During the neoplastic transformation, mammary epithelial cells undergo alterations in their gene expression patterns (Allinen et al., 2004). Unfortunately, it has not been possible to identify distinct markers to predict this transformation from *in situ* to invasive disease (Yeong et al., 2017). DCIS-associated ME cells display immunophenotypic differences in comparison to ME cells surrounding normal structures. Several markers, such as basal CKs, α-SMA, SMMHC, calponin, p63, p75, maspin, WT-1, and CD10 have been demonstrated to decrease prior to the invasive stage (Chocteau et al., 2019; Guelstein et al., 1993; Hilson et al., 2009; Kalof et al., 2004; Rohilla et al., 2015;Werling et al., 2003; Wetzels et al., 1989; Zhang et al., 2003). A sequential disappearance has been shown for p63, calponin, and α-SMA. The loss of α-SMA expression is linked to later events, and taking place just before invasion (Russell et al., 2015). Recently, loss of α-SMA was also shown to compromise the barrier made by ME cells (Sirka et al., 2018), suggesting that the ME layer acts as a mechanical barrier and that the contractile potential, mediated by α-SMA, is important for its protective function. Besides displaying physical hindrance, ME cells are known to participate in the production of BM and regulation of matrix metalloproteinases, further supporting their importance against invasion (Gudjonsson et al., 2002; Jones et al., 2003; Sánchez-Céspedes et al., 2016; Sarper et al., 2017). Alterations in DCIS-associated ME cells have been demonstrated by gene expression profiling (Allinen et al., 2004). However, the mechanisms behind the disruption of the ME layer during malignant progression are not well understood.

To better understand the role of an intact ME cell layer and mechanisms behind its maintenance, we have utilized a comparative canine mammary tumor model for human breast carcinomas. Canine and human mammary tumors share similarities in their epidemiology, etiology, histomorphology, biological behavior, and molecular biology. In addition, most mammary carcinomas in humans and canines represent malignant hyperplasias of ductal epithelial cells (Goldschmidt et al., 2011; Klopfleisch et al., 2011; Rasotto et al., 2014; Rivera and von Euler, 2011; Sorenmo et al., 2011; Uva et al., 2009). Using immunohistochemistry, we compared expression patterns of basal/ME markers in untransformed canine mammary tissue sections with non-invasive intraductal epithelial proliferative lesions of UDH, ADH, and DCIS. We observed that in the basal/ME cells the expression of cytoskeletal proteins α-SMA, CK5, and CK14 slightly responded to intraductal proliferations according to the ductal segment and type of proliferative lesion. At the invasive stage, the expression of these specific markers was absent, coinciding with the disruption of the intact ME cell layer. Furthermore, our cell biological experiments with primary canine mammary epithelial cells and the human mammary epithelial cell line showed that the loss of CK5, and to a lesser extent CK14, from the basal progenitor population affected maturation of the progenitors into functional, contractile ME cells. Simultaneously, a differentiation bias toward the luminal epithelial cell type was detected with loss of normal 3D mammosphere morphology and reduction in the basement membrane protein laminin-5. Importantly, loss of CK5 was associated with downregulation of transcriptional repressor Zinc finger protein SNAI2 (SLUG), an important regulator of the mammary epithelial cell lineage determination. In conclusion, our data suggest that CK5 impacts lineage specific differentiation and in this way may direct the formation of a normal ME layer, subsequently affecting the maintenance of a normal BM layer and mammary organostructural homeostasis. Hence, our findings expand our understanding of the carcinogenetic mechanisms at the pre-invasive stage and the development of phenotypic heterogeneity in mammary carcinomas.

## RESULTS

### Basal/myoepithelial markers CK5, CK14 and α-SMA display specific expression patterns according to ductal segment and type of intraductal hyperplasia

In women and female canines, invasive mammary carcinomas have been proposed to originate from the terminal duct lobular unit (TDLU). The TDLU comprises a lobule with acini (terminal ductules) and intralobular terminal duct together with an extralobular terminal duct, which drains into a larger interlobular duct (Figure S1A). In these structures, ME cells display spatial differences in their morphology and immunophenotype, and molecular alterations have been demonstrated in DCIS-associated ME cells (Allinen et al.,

2004; Chocteau et al., 2019; Hilson et al., 2009; Rønnov-Jessen et al., 1996; Russell et al., 2015; Sánchez-Céspedes et al., 2016).

To establish these observations quantitatively, we first determined the 3.3′-diaminobenzidine-tetrahydrochloride (DAB) chromogen staining intensity (DABi) values for the basal/myoepithelial markers CK5, CK14 and α-SMA from normal intralobular terminal ductal segments and extralobular terminal/interlobular ductal segments using scanned immunohistochemical canine mammary tissue serial sections (Figures S3A and S3B). Slight but statistically significant difference was observed between the ductal segments for α-SMA, with normal intralobular terminal ducts showing lower DABi values in comparison to extralobular terminal/interlobular ductal segments. However, the DABi values for CK5 and CK14 were not statistically significant between different segments (Figure S1B). Hence, our data demonstrate quantitatively that the expression pattern of basal/ME marker α-SMA differs in a spatial manner in the normal ductal segments.

α-SMA, CK5, and CK14 are known to be lost from the basal/ME layer prior to the invasive stage (see e.g. Rohilla et al., 2015; Russell et al., 2015; See also Figure 1A for α-SMA example). To evaluate how the expression of these proteins is altered with an increasing grade of malignancy, we explored the DABi of these markers in non-invasive intraductal proliferative lesions of UDH, ADH and various grades of DCIS, and compared them to one another and to the normal ductal segments in the same canine patients (Figures 1B, 1C,S2A, and S2B). This analysis showed that in the extralobular terminal/interlobular ducts, statistically significant difference can be determined only for CK5 with I-G DCIS values slightly lower than in the corresponding normal ducts (Figure 1C).

In the intralobular terminal ductal segments CK5 exhibited lower values in florid UDH compared to normal and higher values in I-G DCIS compared to florid UDH. Lower values were determined for α-SMA in normal compared to I-G DCIS, and in mild-to-moderate UDH compared to I-G DCIS. CK14 values did not show statistically significant differences (Figure S2B). Taken together, these data show slight spatial differences in the expression of ME marker α-SMA between the normal ductal segments. The other comparative results suggest that cytoskeletal CK5 and α-SMA in the basal/ME layer may respond to non-invasive intraductal proliferative lesions in a spatial- and lesion-type-dependent manner.

### Loss of α-SMA, CK5 and CK14 leads to abnormal 3D mammosphere formation

In both humans and canines, CKs 5 and 14 as well as α-SMA are expressed in the mammary basal/ME layer, but lost upon invasion (see e.g. Rohilla et al., 2015; Russell et al., 2015; Chocteau et al., 2019; Figure 1A). To understand how the loss of these specific markers would contribute to the properties of the ME layer and to the overall morphology of mammary epithelial structures, we isolated $CD24^{+}$ -epithelial cells with fluorescence-activated cell sorting (FACS) from primary canine mammary organoids (Figures S3C–S3F). The isolated population comprised of basal and luminal cells (Figure S3G) (Sleeman et al., 2006). These primary epithelial cells were targeted with CK5, CK14, or α-SMA-specific siRNAs in 3D Matrigel cultures (Figures 2A and S4A). Loss of each of these proteins led to significantly altered mammosphere morphology with a larger diameter (Figures 2A and 2B). Furthermore, we depleted these proteins from human MCF10A mammary epithelial cells, containing both basal and luminal cell types (Krause et al., 2008; Bhat-Nakshatri et al., 2010; Sarrio et al., 2012; Liu et al., 2014; Sokol et al., 2015; Qu et al., 2015; Miller et al., 2018). As these cells in long-term 3D cultures express markers against both luminal and basal/ME cells and produce laminin-5 to the forming basement membrane (Figures 2C and S4B; See also refs. Debnath et al., 2003; Gaiko-Shcherbak et al., 2015; Pinto et al., 2011; Qu et al., 2015; Pseftogas et al., 2020), we found this cell line as a useful model to target basal/ME proteins. Similar to canine mammary epithelial cells, loss of CK5, CK14, or α-SMA from human mammary epithelial cell cultures by specific siRNAs led to significantly enlarged mammosphere structures of abnormal morphology (Figures 2D and 2E).

To further explore whether the loss of these specific CKs could affect the morphology of 3D structures by impacting the epithelial differentiation process, we isolated the $CD49f^{+}$ $EpCAM^{-}$ population (Eirew et al., 2008; Stingl et al., 2001), enriched for basal progenitors, from the MCF10A cell line (Figures S4C–S4E). These progenitor cells were targeted by lentiviral-based RNA interference to knock down CK5 and CK14 (Figures S4F, S4G, and S5A). Similar to siRNA experiments these knock down (KD) cells in a 3D environment formed larger mammospheres with abnormal morphology (Figures 2F,S5B, and S5C). These results

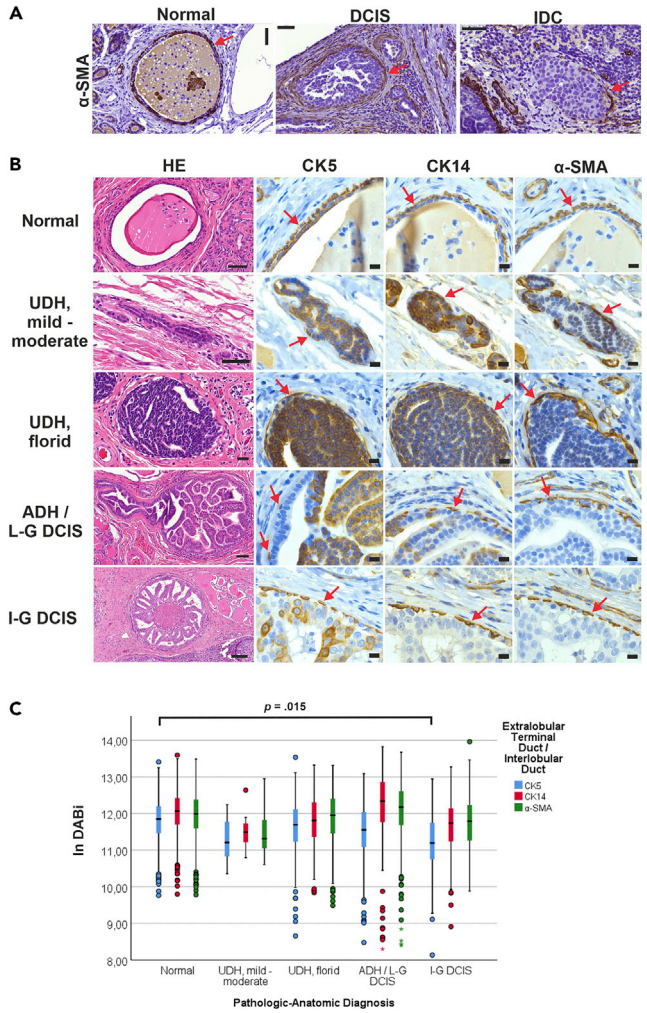


**Figure 1. Intraductal hyperplasia in the extralobular terminal duct/interlobular ductal segment is associated with modest basal myoepithelial response that is lost prior to invasive stage**

(A) Loss of myoepithelial cell layer prior to invasive stage. Canine mammary myoepithelial layer visualized with immunohistochemical staining for α-SMA (red arrows) in normal interlobular duct (left), ductal carcinoma *in situ* (DCIS; middle) and invasive ductal carcinoma (IDC; right). Bar 50 μm.

(B) Consecutive canine mammary FFPE tissue sections of normal, mild-to-moderate usual ductal hyperplasia (UDH, mild-moderate), florid usual ductal hyperplasia (UDH, florid), atypical ductal hyperplasia (ADH), low-grade ductal carcinoma *in situ* (L-G DCIS) and intermediate-grade ductal carcinoma *in situ* (I-G DCIS) were stained using hematoxylin-eosin (HE, far left) and the basal myoepithelial markers CK5 (middle left), CK14 (middle right) and α-SMA (far right). Representative images of the lesions are shown. Red arrows indicate basal myoepithelial layer as distinct from intraluminal cellular hyperplasia. Bar for HE in normal and mild-to-moderate UDH 50 μm, florid UDH 20 μm, ADH/L-G DCIS 50 μm, I-G DCIS 100 μm and in all IHC 10 μm.

(C) Boxplot of the extralobular terminal / interlobular ductal cellular ln-transformed DAB chromogen staining intensity (DABi) values for normal CK5 n(cells) = 1203, CK14 n = 1469, α-SMA n = 1765; mild-to-moderate UDH CK5 n(cells) = 12, CK14 n = 12, α-SMA n = 16; florid UDH CK5 n(cells) = 248, CK14 n = 403, α-SMA n = 304; ADH/L-G DCIS CK5 n(cells) = 268, CK14 n = 383, α-SMA n = 383; I-G DCIS CK5 n(cells) = 203, CK14 n = 258, α-SMA n = 319. Canine patient n = 7. Black middle line within box represents median. Height of box is interquartile range (IQR), representing 75$^{th}$ and 25$^{th}$ percentiles, respectively. Whiskers represent the lowest and highest data within the 1.5 x IQR of the lower and upper quartiles, respectively. Circles represent outliers. Linear mixed model with random intercepts for canine individual and ductal segment was used. Pairwise comparison over all the individual companions was implemented with Bonferroni's multiple comparisons correction. The level of significance was defined as $p < 0.05$. Only statistically significant mean differences are indicated. CK5 expression was significantly decreased in I-G DCIS compared to normal ($p = 0.015$). See also Figures S1–S3.

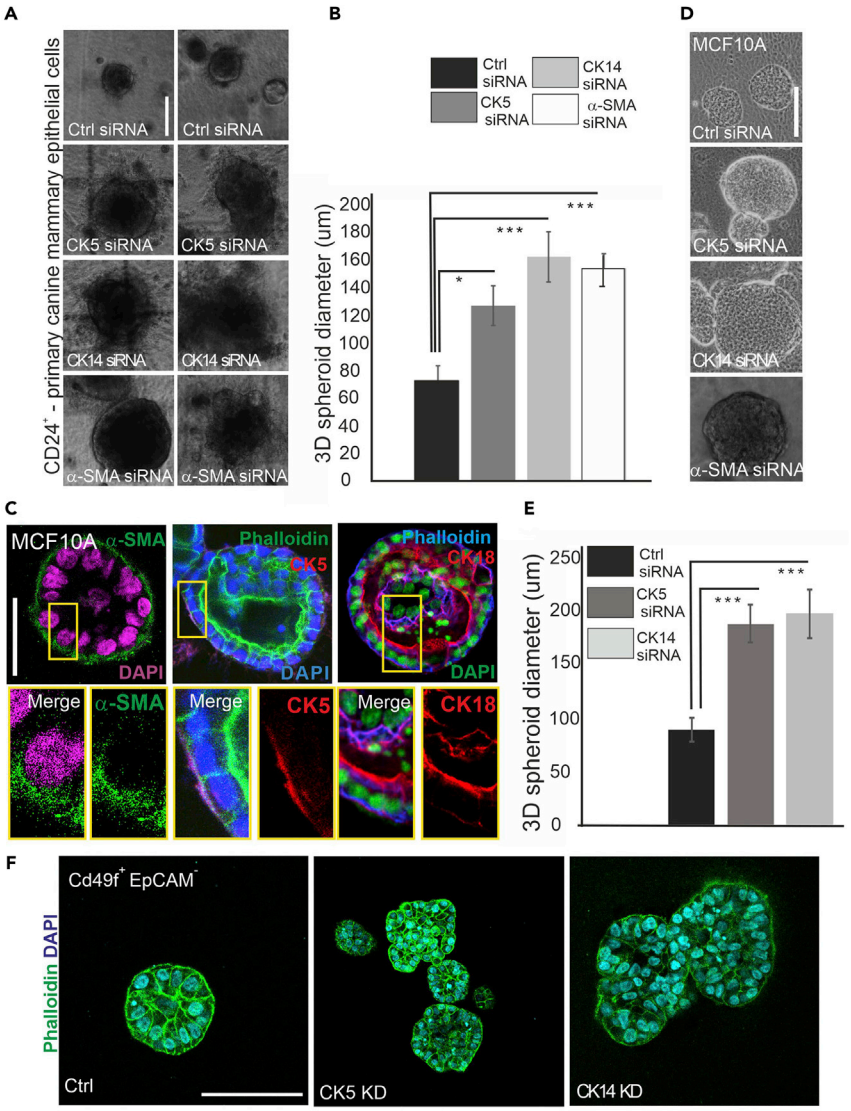


**Figure 2. Loss of CK5, CK14 or α-SMA affects the homeostasis of mammary epithelial structures**

(A) Depletion of primary canine mammary epithelial cells ($CD24^+$) by specific siRNAs against CK5, CK14, and α-SMA in 3D Matrigel. Two panels of representative bright field images after 2 weeks of culture are shown. Bar 100 μm.

(B) Quantification of canine 3D mammary organoid diameters from ctrl, CK5-, CK14-, and SMA-depleted samples, related to Figure 3A. Mean (±SEM) is shown; n(ctrl) = 31, n(CK5 siRNA) = 51, n(CK14 siRNA) = 31, n(α-SMA siRNA) = 33 ***P<0.001 (Mann–Whitney–Wilcoxon rank-sum test).

(C) 3D-structures of MCF10A cells in Matrigel display both luminal and basal markers. Human mammary epithelial cells were grown for two weeks in Matrigel, fixed with PFA, and stained with specific antibodies against α-SMA, CK5 and CK18. Phalloidin was used to visualize actin cytoskeleton and DAPI for nuclei. Bar 50 μm.

(D) MCF10A human mammary epithelial cells were depleted for CK5, CK14, and α-SMA by specific siRNAs in 3D Matrigel cultures. Samples were grown for two weeks and fixed with PFA for analyses. CK5- and CK14-depleted mammosphere samples were clearly larger than ctrl 3D structures. Bar 100 μm.

(E) Quantification of the 3D mammosphere diameter from ctrl, CK5- and CK14-depleted samples. Mean (±SEM) is shown; n(ctrl) = 15, n(CK5 siRNA) = 15, n(CK14 siRNA) = 15; ***P<0.001 (Mann–Whitney–Wilcoxon rank-sum test).

(F) Depletion of CK5 and CK14 from 3D cultures $CD49f^+$ $EpCAM^-$/basal progenitor-enriched MCF10A mammary epithelial cell population. Cultures were maintained for two weeks, after which they were fixed with PFA and stained with Phalloidin (green) and DAPI (blue). Representative immunofluorescence images of the 3D mammospheres are shown. Bar 100 μm. See also Figures S3–S5.

indicate that basal/ME proteins CK5, CK14, and α-SMA are important for the maintenance of normal mammary organomorphology, at least in the utilized *in vitro* 3D models.

## Cytokeratin 5 determines maturation of the myoepithelial cells

CKs play a role in the mechanical resistance of epithelial cells (Sanghvi-Shah and Weber, 2017). In line with that, we observed a decrease in the elastic modulus of CK5 KD and CK14 KD cells in comparison to control (CD49f+ EpCAM-/basal progenitor-enriched MCF10A cells) in indentation experiments using an atomic force microscope (AFM). The elastic modulus histograms could be fitted with three Gaussian distributions, revealing a different mechanical behavior at distinct indentation spots within the same cell type (Figures 3A–3D). The elastic modulus values at the peaks of each distribution were significantly lower for CK5 KD and CK14 KD cells when compared with control cells (Figure 3D).

While CK5 and CK14 clearly maintain mechanical properties of the mammary basal/ME layer, it has not been assessed whether they could have additional regulatory roles in the progenitor cells. To understand the role of these CKs in the regulation of mammary progenitor cells, we utilized CD49f$^{+}$ EpCAM$^{-}$/basal progenitor-enriched MCF10A cells that were depleted for CK5 and CK14, and analyzed the expression of several markers by Western blotting (WB) and by immunofluorescence (IF) stainings (Figures 3E–3G and S6A–S6C). The WB results showed that CK5 KD cells, and to a lesser extent CK14 KD cells, displayed decreased levels of ME cell marker α-SMA, while the luminal epithelial marker CK18 was slightly increased in CK5 KD cells and the luminal epithelial marker CK19 decreased (Figures 3E–3G and S6A–S6C). Additionally, CK5 KD cells displayed lower levels of ME cell markers vimentin, smooth muscle myosin heavy chain (SMMHC) and calponin 1 (Figures S6B and S6C). Similar results showing downregulation of vimentin and α-SMA were obtained by utilizing specific siRNAs against CK5 in MCF10A cell line (Figures 3H and 3I). In addition, we performed combined CK5/CK14 siRNA experiments, but could not see higher depletion of α-SMA upon the combined siRNA treatment in comparison to CK5 depletion alone (Figures S6D and S6E). Interestingly, depletion of α-SMA seemed to reciprocally downregulate CK5 and vimentin, indicating a feedback loop mechanism in between these proteins (Figures S6F and S6G). These results suggest that CK5 has a major role in the maturation process of ME cells, the loss of CK5 leading to a differentiation bias toward the CK18$^{+}$ luminal epithelial cell type. As CK5 and CK14 are known to heterodimerize, it may also be possible that the milder impact of CK14 depletion goes through CK5.

## Loss of Cytokeratin 5 impairs junctional integrity and affects deposition of basement membrane proteins

CKs are linked to integrin- and cadherin-based adhesions, and have been associated with regulation of these cell adhesive structures (Sanghvi-Shah and Weber, 2017). As CK5, and to a lesser extent CK14, were found to affect the maturation of ME cells, we wanted to assess whether loss of these proteins could also impact the resistance of the ME layer through cell adhesive structures. The levels of the ME-specific cell-cell contact proteins Dsg3 and P-cadherin (Daniel et al., 1995; Runswick et al., 2001) were determined from lysates of both ctrl (CD49f$^{+}$ EpCAM$^{-}$/basal progenitor-enriched MCF10A cells) and the corresponding CK5 and CK14 KD cell lines (Figures 4A and 4B). Both markers were significantly decreased upon loss of CK5, while loss of CK14 did not seem to play a role in maintaining their levels (Figures 4A and 4B). More detailed immunofluorescence analyses of Dsg3-stained fully confluent epithelial monolayers revealed that Dsg3 partially lost its junctional pattern in CK5-deficient cells and that the cell-cell junctions appeared less mature, with spiky protrusions (Figures 4C and 4D). In a 3D environment, CK5 KD cells displayed lower Dsg3-staining pattern, while CK14 KD cells had many randomly localized cells with junctional Dsg3 within the morphologically abnormal 3D structures (Figure S7A). Staining of luminal marker E-cadherin from 3D mammospheres was, however, prominent in all samples but the distribution of E-cadherin positive cells in CK5 and CK14 KD spheroids was clustered and abnormal in comparison to the ctrl 3D mammospheres (Figures 4E and 4F). As with CK5 loss, slight decrease in Dsg3 and P-cadherin levels was detected upon α-SMA-depletion by siRNA in MCF10A cells (Figure 4G). These data indicate that CK5 may play a role in the integrity of ME cell junctions at least through P-cadherin and Dsg3, and that bidirectional signaling within the basal/ME layer may be important for the overall maintenance of the epithelial cell populations.

As CK5 loss affected cell-cell adhesions, we further studied whether its downregulation would play a role in the regulation of cell-substrate adhesions. Immunofluorescence stainings with vinculin antibody in ctrl (CD49f$^{+}$ EpCAM$^{-}$/basal progenitor-enriched MCF10A cells) or CK5-deficient cells showed slightly more prominent vinculin-based cell-substrate adhesions, while vinculin at the cell-cell contacts was showing

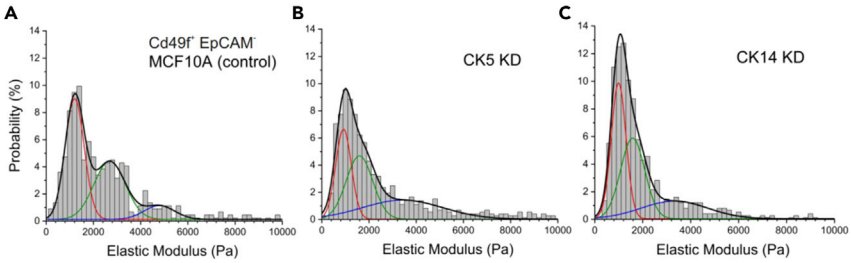


D

| Cell types | Elastic modulus (Pa) | | |
|---|---|---|---|
| | Peak of first Gauss distribution | Peak of second Gauss distribution | Peak of third Gauss distribution |
| MCF10A (control) | 1210 ± 30 | 2690 ± 80 | 4800 ± 300 |
| CK5 KD | 918 ± 20 | 1590 ± 170 | 3400 ± 300 |
| CK14 KD | 990 ± 30 | 1600 ± 400 | 3300 ± 700 |

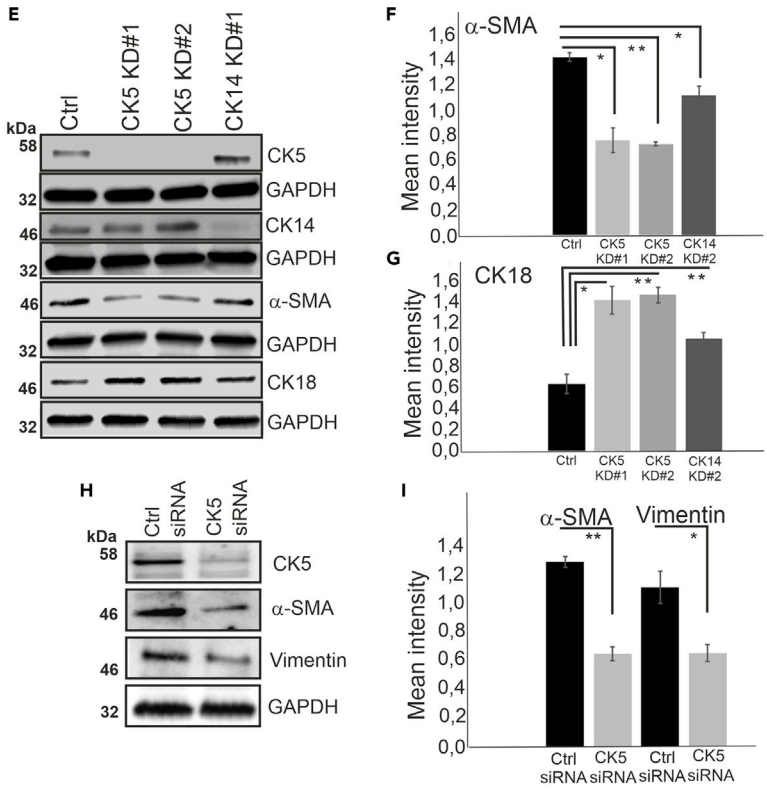


**Figure 3. Loss of CK5 affects maturation of myoepithelial cells**

(A–C) Elastic moduli of cells determined in cell indentation experiments by AFM. Elastic modulus histograms for (A) Control (CD49f$^{+}$ EpCAM$^{-}$ -enriched basal progenitors from MCF10A cells), (B) CK5 KD cells and (C) CK14 KD cells. The histograms were fit with 3 Gaussian distributions (black lines). Each Gaussian distribution is shown separately (red, green, and blue lines).

(D) Elastic modulus values for the peaks of the Gaussian distributions of Control (CD49f$^{+}$ EpCAM$^{-}$ -enriched basal progenitors from MCF10A cells), CK5 KD, and CK14 KD cells.

(E) Western blot analyses on cell lysates from ctrl and CK5-and CK14-depleted cell lines showed downregulation of α-SMA, as detected by specific antibody. In contrast, luminal marker CK18 was slightly elevated in the corresponding cell lysate samples.

(F and G) Quantification of the α-SMA and CK18 Western blot experiments. Mean (±SEM) is shown; n = 3; *P<0.05, **P<0.01 and ***P<0.001 (paired ttest).

(H) Ctrl siRNA-treated MCF10A cells and MCF10A cells depleted for CK5 siRNA were analyzed in Western blotting by specific antibodies against α-SMA and vimentin. GAPDH was used as a loading control.

(I) Quantifications of the Western blots, related to Figure 3H. Mean (±SEM) is shown; n = 3; *P<0.05 and **P<0.01 (paired ttest). See also Figure S6.

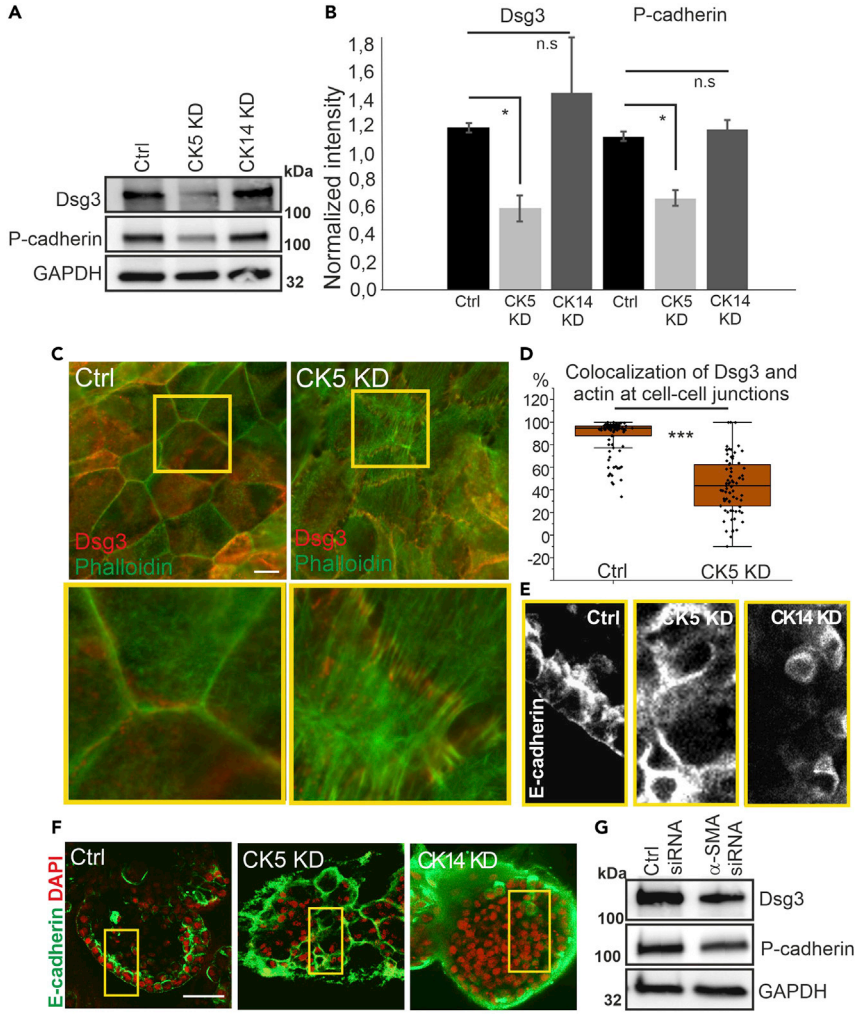


**Figure 4. Loss of CK5 affects cell-adhesive structures**

(A) Western blot analyses on cell lysates from ctrl and CK5-and CK14-depleted cell lines showed downregulation of Dsg3 and P-cadherin upon loss of CK5 but not CK14. GAPDH is used as a loading control.

(B) Quantification of the Dsg3 and P-cadherin Western blot experiments, related to Figure 4A. Mean (±SEM) is shown. n = 4 *P<0.05 (paired ttest); n.s.= not significant.

(C) Ctrl ($CD49f^+$ $EpCAM^-$, enriched for basal progenitors) and CK5 KD cells were used in immunofluorescence microscopy of fully-confluent monolayer cultures. Specific antibody against Dsg3 was used. Actin cytoskeleton was visualized with Phalloidin and nuclei were stained with DAPI. Magnifications of the cell-cell junction areas, indicated with yellow boxes, are shown below. Bar 20 μm.

(D) Quantification of the colocalization in between Dsg3 and actin at cell-cell junctions. n(ctrl) = 91, n(CK5 KD) = 75. The amount of colocalization (%) is shown as box plot with inner and outlier points and mean. ***P<0.001 (paired ttest).

(E and F) (E) $CD49f^+$ $EpCAM^-$/basal progenitor-enriched MCF10A mammary epithelial cells, CK5 KD and CK14 KD cells were culture in 3D Matrigel for two weeks, after which they were fixed with PFA and stained with E-cadherin. Nuclei were visualized with DAPI. Magnifications of E-cadherin stainings in gray scale are shown in panel (E) and full images with the indicated magnified areas (yellow boxes) are shown below in panel (F). Bar 25 um.

(G) Depletion of α-SMA was performed with specific siRNAs in MCF10A cultures for four days. Cellular lysates from control siRNA and α-SMA siRNA treated cells were used in Western blotting and a specific antibody against Dsg3 was utilized. GAPDH was used as a loading control. See also Figure S7.

punctate, immature type adhesive structures (Figure S7B). As vinculin has an established role in mechano-transduction (Goldmann, 2016), we tested whether cell-exerted forces would be altered in the CK5 KD progenitor cell lines. Traction force imaging experiments showed an increase in the actomyosin-mediated cell-substrate forces in both single cells and monolayers but no changes in the cell doublets (Figures 5, S7C, and

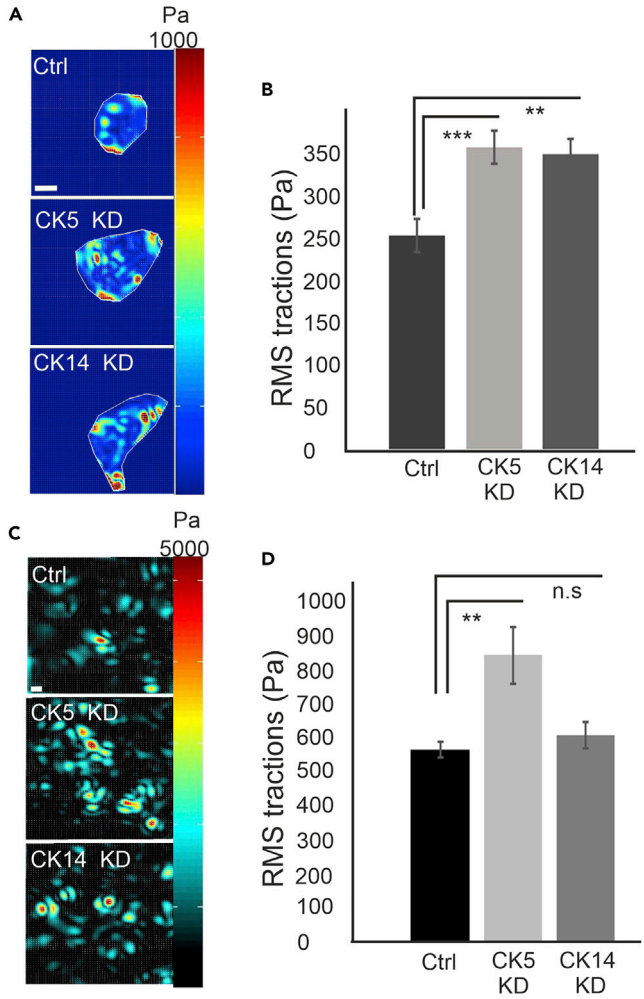


**Figure 5. Loss of CK5 and CK14 impact cellular force production**

(A) Traction force microscopy with ctrl, CK5 KD and CK14 KD cell lines showed altered cell-substrate forces upon CK5 and CK14 depletion. Representative force maps of ctrl, CK5 and CK14 knock-down cells are shown. Bar 20 μm.

(B) Quantification of the traction force microscopy experiments, related to Figure 5A, showed elevated cell-substrate forces upon loss of CK5 and CK14. Mean (±SEM) is shown. n(ctrl) = 32, n(CK14 KD) = 40, n(CK5 KD) = 33; *P<0.05 (Mann–Whitney–Wilcoxon rank-sum test).

(C) Representative examples of monolayer force microscopy maps of ctrl, CK5 KD and CK14 KD cell sheets. Bar 40 μm.

(D) Quantification of the monolayer force microscopy experiments, related to Figure 5C, showed elevated cell-substrate forces upon loss of CK5. Mean (±SEM) is shown. n(ctrl) = 19, n(CK5 KD) = 16, n(CK14 KD) = 16; **P<0.01; n.s= not significant (Mann–Whitney–Wilcoxon rank-sum test). See also Figure S7.

S7D). These results indicate that the lack of CK5 and CK14 may be counteracted by the redistribution of intercellular forces, and that loss of these cytokeratins may lead to redistribution of cellular forces.

Finally, to reveal whether CK5 could impact the barrier against transformed luminal cells also through basement membrane formation, we stained 3D mammosphere cultures with laminin-5. Fully mature MCF10A acinar structures in 3D are known to produce laminin-5 to the basement membrane (Gaiko-Shcherbak et al., 2015). While we detected this layer both in MCF10A and Cd49f+ EpCAM-cultures (Figures S4B and 6A), CK5 deficient cultures were displaying significantly decreased amounts of laminin-5 around the spheroids as visualized by the intensity maps of laminin-5-stainings (Figures 6A,6B, andS8A). However, CK14 KD cultures did not alter significantly from the ctrl cultures. Additionally, decreased levels of laminin-5 were detected in Western blot experiments, performed from CK5 siRNA-treated MCF10A cells (Figures S8B and S8C). These results act as additional proof for the observations that loss of CK5 not only

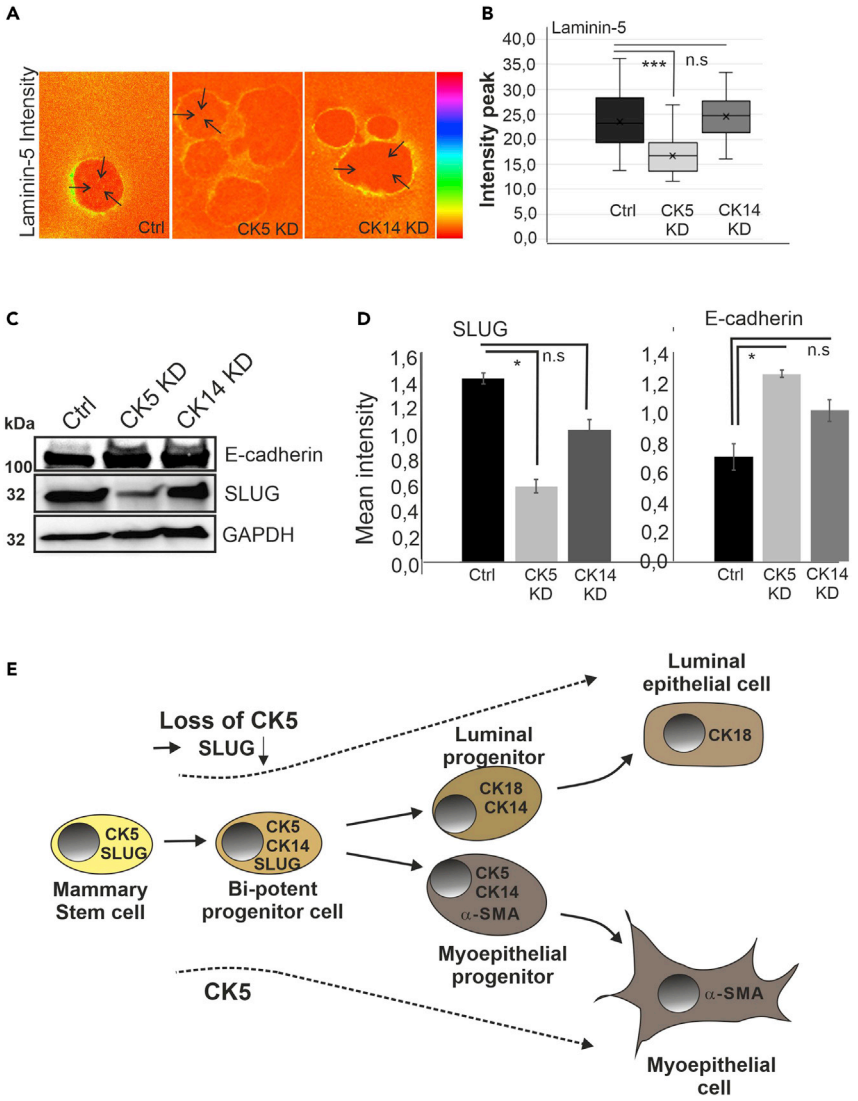


**Figure 6. Depletion of CK5 affects laminin-5 production and Zinc finger protein SNAI2 (SLUG2) levels**

(A) CD49f$^{+}$ EpCAM$^{-}$/basal progenitor-enriched MCF10A mammary epithelial cells, CK5 KD and CK14 KD cells were culture in 3D Matrigel for two weeks, after which they were fixed with PFA and stained with laminin-5 (See also Figure S8A). Intensity maps were created in Fiji. Lineprofiles were drawn from the edge of the spheroid toward the center. 3–5 lineprofiles were drawn on each spheroid for the analyses of laminin-5 intensity.

(B) Peak values on point 3 from lineprofiles were utilized for further analyses. Values for ctrl, CK5 and CK14 peak values from line profiles are shown in box plots with inner and outlier points and mean. n(ctrl)= 30; n(CK5 KD) = 57; n(CK14 KD) = 33. ***P<0.001 (paired ttest). (ttest, two tailed, equal variance).

(C) Western blot analyses on cell lysates from ctrl and CK5- as well as CK14-depleted cell lines showed downregulation of SLUG and slight upregulation of E-cadherin upon loss of CK5, as detected by specific antibody. GAPDH was used as a loading control.

(D) Quantification of SLUG and E-cadherin Western blot experiments. Mean (±SEM) is shown; n = 3; *P<0.05; n.s.= not significant (paired ttest).

(E) A hypothetical model for the role of CK5 in the differentiation of mammary epithelial cell lineages, possibly through the regulation of SLUG. Some of the markers involved in this study are shown as examples within specific cell populations. Note that in the interest of space, several markers are missing from the hypothetical model and that in this study we did not concentrate on the expression pattern of these markers in distinct differentiation phases of the mammary epithelial cell populations. See f.i. Böcker et al. (2002); Boecker and Buerger (2003); Villadsen et al. (2007); Boecker et al. (2018); Fu et al. (2020) for such studies. See also Figure S8.

impacts the mechanical features of the basal layer but also leads to loss of protective basement membrane possibly through impaired maturation of myoepithelial cells.

### Loss of CK5 leads to downregulation of SLUG

To further assess the mechanisms through which CK5 and CK14 could impact the differentiation of mammary epithelial cells, we analyzed the levels of SLUG, a master regulator of the mammary epithelial cell lineage determination and normal tubulogenesis (Nassour et al., 2012; Phillips et al., 2014). In CK5, and to a lesser extent in CK14-deficient cells, SLUG was downregulated (Figures 6C and 6D). In line with these observations, the level of E-cadherin, a known target for SLUG-mediated repression (Bolós et al., 2016), was slightly upregulated upon depletion of CK5 (Figures 6C and 6D). Furthermore, depletion of CK5 by specific siRNAs from MCF10A mammary epithelial cells led to similar results and, additionally, loss of α-SMA by siRNA had an almost equal impact (Figures S8D–S8F), again indicating reciprocal regulation within the basal cell populations. It should be noted that long-term downregulation of CK5 in cell culture conditions leads to upregulation of some other cytokeratins, including CK6, indicating that loss of CK5 is compensated through an alternative mechanism. This is supported by the re-induction of the studied myoepithelial markers and upregulation of several cytokeratins in the long-passaged cell clones (Figure S9).

These data indicate that the loss of CK5 may lead to differentiation bias in the mammary progenitors through regulation of SLUG levels. How specifically CK5 impacts SLUG levels, needs to be assessed in future studies. A hypothetical model for CK5 in the regulation of mammary epithelial lineage differentiation and formation of an intact, functional ME layer is presented in Figure 6E.

## DISCUSSION

Mammary myoepithelial cells are important for normal mammogenesis and organostructural homeostasis, and have additionally been shown to have tumor suppressive properties (Gudjonsson et al., 2002; Jones et al., 2003; Polyak and Hu, 2005; Sánchez-Céspedes et al., 2016). Absence of ME cells and BM penetration determines stromal invasion, and a gradual loss of ME markers has been suggested to concur with malignant transformation of intraductal epithelial cells with subsequent breakdown of the protective ME barrier (Hilson et al., 2009; Kalof et al., 2004; Rohilla et al., 2015; Russell et al., 2015; Werling et al., 2003; Zhang et al., 2003). However, the molecular mechanisms behind the maintenance of this suggested myoepithelial barrier function are still poorly understood.

In this study, our goal was to understand in more detail the mechanisms leading to compromised ME barrier function. For this, we used a comparative canine model with immunohistochemical serial stainings for CK5, CK14, and α-SMA. With these markers we were able to demonstrate some alterations in the basal/ME layer, in non-invasive intraductal proliferations of increasing grade of malignancy (UDH, ADH/L-G DCIS, I-G DCIS) by quantitatively determining their DAB chromophore staining intensity values in the TDLU and efferent interlobular ducts (Figures 1C and S2B). Of these markers, only α-SMA displayed spatially statistically different expression patterns within the normal mammary ductal segments (Figure S1B). This result is in line with previous reports which have made semi-quantitative estimates on differences between the lobular alveolar/ductal and extralobular ductal compartments in the expression of some basal/ME markers in normal human mammary epithelium (e.g. Chen et al., 2015; Foschini et al., 2000; Pusztaszeri, 2010). This observation is possibly connected to the compartmentalization of the mammary epithelial structures into the intralobular functional alveolar and proliferative ductal zones and the extralobular efferent ductal system (Böcker et al., 2002; Rønnov-Jessen et al., 1996; Pusztaszeri, 2010). The impact of the differential composition of the surrounding intra- and extralobular stromal tissue on the segment-specific expression pattern should be further investigated.

Furthermore, we showed that the expression patterns of CK5 and α-SMA of the basal/ME layer in the canine intralobular terminal ductal segments and the extralobular terminal/interlobular ductal segments undergo modest changes upon non-invasive intraductal proliferations (Figures 1C and S2B). In the extralobular terminal/interlobular ductal segment, the expression of these markers appears to slightly decrease already in the intermediate-grade DCIS prior to the invasive stage and is eventually lost at invasion (Figures 1A–1C). What is the biological significance or whether the cytoskeletal markers respond to non-invasive intraductal epithelial proliferations needs further studies.

α-SMA is lost from the basal/ME layer prior to invasion (Russell et al., 2015). A recent study suggested that expression of α-SMA, mediating the contractile properties of the ME layer, is essential for the mechanical barrier

function of ME cells against an invasion of transformed epithelial cells (Sirka et al., 2018). Our experiments showed that depletion of α-SMA from the basal layer in 3D cultures led to abnormal mammosphere morphology (Figure 2), supporting the observation that contractility and mechanical features of the ME layer are crucial for the maintenance of normal mammary organostructure. Interestingly, loss of CK5 and CK14 from the basal layer resulted in similar, abnormally large and irregular 3D morphology (Figures 2, S5B, and S5C). Since cytokeratins are important for the mechanical features of epithelial cells, as also shown in our cell indentation experiments (Figures 3A–3D), KD of CK5 and CK14 could lead to abnormal compliancy of the basal layer and in this way advance such drastic morphological defects in the 3D mammospheres.

CK5 and CK14 are expressed in mammary stem and progenitor cell populations (Böcker et al., 2002; Boecker et al., 2018; Lee et al., 2012; Villadsen et al., 2007). However, their functions in the progenitors are not properly understood. Here, we show that KD of CK5, and to a lesser extent of CK14, affected the lineage commitment of the mammary progenitors: CK5-depleted CD49f$^{+}$ EpCAM$^{-}$/basal progenitor-enriched cells showed impaired maturation into contractile ME cells, which was indicated by lower levels of α-SMA, vimentin, SMMHC and calponin 1, and a concurrent increase in the expression of CK18 (Figures 3 and S6). Loss of CK14 had in our studies only a slight effect on these ME cell markers (Figures 3 andS6) and, as it is known to heterodimerize with CK5, this slight effect could possibly also go through CK5.

Additionally, ME-specific cell-cell junction proteins P-cadherin and Dsg3 were downregulated upon loss of CK5, causing deficiency in the maintenance of intact epithelial structures (Figure 4). Spatially selective expression of P-cadherin in mammary ME layer is required for the integrity of epithelial tissues and normal mammary architecture, and it has been shown that KD of P-cadherin from the ME cells compromises the barrier function of this cell layer (Idoux-Gillet et al., 2018; Sirka et al., 2018; Vieira et al., 2014). Furthermore, Dsg3 has been shown to co-localize with CK5 and CK14 and is linked to mechanotransduction through E-cadherin complex, indicating a role for this cell junction protein both in the maintenance of epithelial integrity and in adjustment of mechanical resistance in response to increasing external forces (Uttagomol et al., 2019; Vielmuth et al., 2018). Loss of CK5 from the basal progenitors thus affects the compliance, contractility, and integrity of the epithelial junctions, clearly leading to loss of ME barrier function. Interestingly, loss of α-SMA from the ME cells also led to downregulation of CK5, vimentin, and Dsg3, indicating a regulatory feedback loop mechanism in between CK5 positive stem/progenitor cells and mature ME cells (Figures 4G,S6F and S6G). Furthermore, as CK5 KD led to impaired production of basement membrane protein laminin-5 around the 3D mammospheres (Figures 6A,6B, and S8A–S8C), the results indicate that CK5 not only impacts the mechanical features of the basal layer but also affects barrier function through the regulation of basement membrane, which is deposited by mature myoepithelial cells.

As α-SMA has been suggested to be the main protein to mediate the contractile potential of ME cells (Haaksma et al., 2011), we expected that loss of the mature ME cell phenotype would lead to a cell type which exerts less forces on its environment. However, actomyosin-mediated cell-substrate forces were slightly increased, as detected by traction force microscopy with single cells and also with monolayers (Figures 5,S7C, and S7D). This may be explained by the lower levels of these specific cytokeratins as well as the subsequent lower levels of vimentin, since intermediate filaments have been indicated to play a role in the co-regulation of actomyosin forces through their association with cell adhesion sites (Bordeleau et al., 2010, 2012; Jiu et al., 2017). The KD phenotype could thus exert uncontrolled forces on the underlying substrate. Alternatively, weakened cell-cell junctions and the appearance of more prominent cell-substrate adhesions in the KD cell lines could result in redistribution of cellular forces more toward the underlying substrate. Whether this has an impact on cellular motility needs to be further assessed in the future.

Finally, the loss of mature ME cell phenotype upon CK5 KD was associated with slightly higher expression of luminal marker CK18 (Figures 3 and S6), indicating a differentiation bias towardthe luminal cell type. CK5-deficient cells also expressed significantly lower levels of the transcriptional repressor SLUG (Figures 6C, 6D, and S8D–S8F). SLUG has been shown to determine the lineage specific differentiation of mammary epithelial cells and is co-localized in a subpopulation of basal cells together with CK5, P-cadherin, and CD49f (Nassour et al., 2012). In line with our observations, SLUG-deficient cells have been shown to overexpress higher levels of markers linked to luminal lineage, such as CK8, CK18, and ER (Nassour et al., 2012). SLUG-deficient adult mice display abnormal mammary epithelial cell lineage differentiation with increased expression of luminal markers in the basal layer and hyperplasia of luminal cells (Phillips et al., 2014). Supporting that, our studies showed that CK5 KD, and to a lesser extent CK14 KD cell lines, showed increased

expression of CK18 (Figure 3). In breast cancer, increased CK18 expression has been linked with inhibition of apoptosis, increase in the expression of CK8 and adhesion proteins as well as decrease in vimentin levels (Aiad et al., 2014; Bozza et al., 2018; Bühler and Schaller, 2005; Iyer et al., 2013; Schaller et al., 1996; Weng et al., 2012). Moreover, we observed that E-cadherin, a target for SLUG-mediated repression (Bolós et al., 2016), was upregulated upon depletion of CK5 (Figures 6C,6D,S8D, and S8E). CK5 KD cells were also growing slower and a similar phenotype has been observed in SLUG-deficient cells (Nassour et al., 2012). As SLUG clearly plays a role in the maintenance of basal-like state and represses luminal lineage differentiation, loss of CK5 could conceivably cause the differentiation bias via regulation of SLUG. The exact mechanisms through which CK5 impacts SLUG levels needs to be further studied in the future.

In conclusion, our findings support the previous studies that have underlined the importance of basal myoepithelial cell layer as a barrier that is eventually lost prior to the invasive stage. Our data showed that CK5 loss plays a major role in the disruption of this myoepithelial layer leading to defects in basement membrane formation. Downregulation of CK5 and consequent loss of SLUG led to epithelial cell differentiation bias with subsequent defects in the maturation of myoepithelial cells and a shift toward the CK18-positive luminal epithelial cell type. The reciprocal interactions of these proteins should also be assessed in more detail in the future.

## LIMITATIONS OF THE STUDY

Although this study shows an interesting link between cytokeratin 5 and SLUG expression, possibly playing a role in the differentiation of specific mammary epithelial cell populations, this work does not provide any information on the molecular mechanisms behind this interconnection. The role of CK5 in the regulation of SLUG levels clearly needs further studies in the future. Also, the technical challenges in the 3D mammosphere antibody-stainings limited these studies. Furthermore, the amount of canine patient samples, related to Figure 1, was very limited.

### Resource availability

#### *Lead contact*

Further information and requests for resources and reagents should be directed to and will be fulfilled by the Lead Contact, Sari Tojkander (sari.tojkander@helsinki.fi).

#### *Materials availability*

This study did not generate new unique reagents. Materials are available on request.

#### *Data and code availability*

This study did not generate any unique datasets or code. All raw data is available on request.

## METHODS

All methods can be found in the accompanying Transparent methods supplemental file.

## SUPPLEMENTAL INFORMATION

Supplemental information can be found online at https://doi.org/10.1016/j.isci.2021.102413.

## ACKNOWLEDGMENTS

This work is supported by funding from the Academy of Finland, University of Helsinki, Jane and Aatos Erkko Foundation as well as Sigrid Jusélius Foundation (S.T.), and The Finnish Veterinary Foundation and The Foundation of Veterinary Research (V.D.). The Institute of Biotechnology (HiLIFE Helsinki Institute of Life Science, University of Helsinki, Finland) is acknowledged for the scanning of the IHC stained canine mammary FFPE tissue slides. OutiVapaavuori (Veterinary Teaching Hospital, University of Helsinki, Finland) is thanked for canine mammary tumor samples. LMU imaging unit (HiLIFE Helsinki) is acknowledged for the assistance in imaging-related work and TiinaPessa-Morikawa (Department of Veterinary Biosciences, University of Helsinki, Finland) is thanked for assistance in FACS-related technical aspects. Mona Zimmermann and TuuliaSavela are thanked for the assistance in cell biological assays. Raphael Ahrens is thanked for the assistance in the analysis of AFM indentation curves. This work made use of Aalto University Bioeconomy Facilities, Helsinki, Finland.

## AUTHOR CONTRIBUTIONS

V.D. designed experiments, has collected and diagnosed canine mammary samples, performed IHC staining on FFPE canine mammary samples, collected and analyzed the data for determination of DABi, isolated canine mammary cells with FACS, analyzed and interpreted the data, and prepared Figures 1 andS1–S3 and the manuscript; K.R. has performed siRNA experiments, 3D Matrigel experiments, IF stainings and WBs, contributing to Figures 2, 3, 4, 5, 6, and S3G–S9 and participated in writing the manuscript; S.C. has performed KD cell lines, isolated human mammary cells with FACS, and performed initial WB analyses for Figures 3 and S4; A.A. has participated in the 3D mammary epithelial culture experiments, and Western blot experiments in Figures 2F, 4F, 6A, S5B, S5C, S7A, and S8A–S8C. N.S and R.K. have co-analyzed the traction force data. J.J.V.-D. and M.Ö. have performed AFM experiments and analyses of the data. P.B. has been involved in canine mammary tumor sample collection and provision of clinical patient data; A.S. has been involved in canine mammary tumor sample collection and has provided pathological expertise; S.T. has designed experiments, performed TFM experiments and co-analyzed the data, prepared figures and co-written the manuscript.

## DECLARATION OF INTERESTS

The authors declare no competing interests.

Received: January 15, 2020
Revised: December 6, 2020
Accepted: April 6, 2021
Published: May 21, 2021

## REFERENCES

Aiad, H.A., Samaka, R.M., Asaad, N.Y., Kandil, M.A., Shehata, M.A., and Miligy, I.M. (2014). Relationship of CK8/18 expression pattern to breast cancer immunohistochemical subtyping in Egyptian patients. eCancer *8*, 404.

Allinen, M., Beroukhim, R., Cai, L., Brennan, C., Lahti-Domenici, J., Huang, H., Porter, D., Hu, M., Chin, L., Richardson, A., et al. (2004). Molecular characterization of the tumor microenvironment in breast cancer. Cancer Cell *6*, 17–32.

Arendt, L.M., Keller, P.J., Skibinski, A., Goncalves, K., Naber, S.P., Buchsbaum, R.J., Gilmore, H., Come, S.E., and Kuperwasser, C. (2014). Anatomical localization of progenitor cells in human breast tissue reveals enrichment of uncommitted cells within immature lobules. Breast Cancer Res. *16*, 453.

Arendt, L.M., and Kuperwasser, C. (2015). Form and function: how estrogen and progesterone regulate the mammary epithelial hierarchy. J. Mammary Gland Biol. Neoplasia *20*, 9–25, Review.

Bhat-Nakshatri, P., Appaiah, H., Ballas, C., Pick-Franke, P., Goulet, R., Jr., Badve, S., Srour, E.F., and Nakshatri, H. (2010). SLUG/SNAI2 and tumor necrosis factor generate breast cells with CD44+/CD24- phenotype. BMC Cancer *10*, e411.

Boecker, W., and Buerger, H. (2003). Evidence of progenitor cells of glandular and myoepithelial cell lineages in the human adult female breast epithelium: a new progenitor (adult stem) cell concept. Cell Prolif. *36* (*Suppl. 1*), 73–84.

Boecker, W., van Horn, L., Stenman, G., Stürken, C., Schumacher, U., Loening, T., Liesenfeld, L., Korsching, E., Gläser, D., Tiemann, K., and Buchwalow, I. (2018). Spatially correlated phenotyping reveals K5-positive luminal progenitor cells and p63-K5/14-positive stem cell-like cells in human breast epithelium. Lab. Invest. *98*, 1065–1075.

Bolós, V., Peinado, H., Pérez-Moreno, M.A., Fraga, M.F., Esteller, M., and Cano, A. (2016). The transcription factor Slug represses E-cadherin expression and induces epithelial to mesenchymal transitions: a comparison with Snail and E47 repressors. J. Cell Sci. *116*, 499–511.

Bordeleau, F., Galarneau, L., Gilbert, S., Loranger, A., and Marceau, N. (2010). Keratin 8/18 modulation of protein kinase C-mediated integrin-dependent adhesion and migration of liver epithelial cells. Mol. Biol. Cell *21*, 1698–1713.

Bordeleau, F., Myrand Lapierre, M.-E., Sheng, Y., and Marceau, N. (2012). Keratin 8/18 regulation of cell stiffness-extracellular matrix interplay through modulation of Rho-mediated actin cytoskeleton dynamics. PLoS One *6*, e38780.

Bozza, W.P., Zhang, Y., and Zhang, B. (2018). Cytokeratin 8/18 protects breast cancer cell lines from TRAIL-induced apoptosis. Oncotarget *9*, 23264–23273.

Bühler, H., and Schaller, G. (2005). Transfection of keratin 18 gene in human breast cancer cells causes induction of adhesion proteins and dramatic regression of malignancy in vitro and in vivo. Mol. Cancer Res. *3*, 365–371.

Böcker, W., Moll, R., Poremba, C., Holland, R., van Diest, P.J., Dervan, P., Bürger, H., Wai, D., Diallo, R.I., Brandt, B., et al. (2002). Common adult stem cells in the human breast give rise to glandular and myoepithelial cell lineages: a new cell biological concept. Lab. Invest. *82*, 737–745.

Chen, L., Yin, X., Lu, S., Chen, G., and Dong, L. (2015). Basal cytokeratin phenotypes of myoepithelial cells indicates the origin of ductal carcinomas in situ of the breast. Appl. Immunohistochem. Mol. Morphol. *23*, 558–564.

Chocteau, F., Abadie, J., Loussouarm, D., and Nguyen, F. (2019). Proposal for a histological staging system of mammary carcinomas in dogs and cats. Part 1: canine mammary carcinomas. Front. Vet. Sci. *6*, 388.

Collins, L.C., Tamimi, R.M., Baer, H.J., Connolly, J.L., Colditz, G.A., and Schnitt, S.J. (2005). Outcome of patients with ductal carcinoma in situ untreated after diagnostic biopsy: results from the Nurses' Health Study. Cancer *103*, 1778–1784.

Daniel, C.W., Strickland, P., and Friedmann, Y. (1995). Expression and functional role of E- and P-cadherins in mouse mammary ductal morphogenesis and growth. Dev. Biol. *169*, 511–519.

Debnath, J., Muthuswamy, S.K., and Brugge, J.S. (2003). Morphogenesis and oncogenesis of MCF-10A mammary epithelial acini grown in three-dimensional basement membrane cultures. Methods *30*, 256–268.

Eirew, P., Stingl, J., Raouf, A., Turashvili, G., Aparicio, S., Emerna, J.T., and Eaves, C.J. (2008). A method for quantifying normal human mammary epithelial stem cells with in vivo regenerative ability. Nat.Med. *14*, 1384–1389.

Foschini, M.P., Scarpellini, F., Gown, A.M., and Eusebi, V. (2000). Differential expression of myoepithelial markers in salivary, sweat and mammary glands. Int. J. Surg. Pathol. *8*, 29–37.

Fridriksdottir, A.J., Villadsen, R., Morsing, M., Klitgaard, M.C., Kim, J., Petersen, O.W., and Rønnov-Jessen, L. (2017). Proof of region-specific multipotent progenitors in human breast

epithelia. Proc. Natl. Acad. Sci. U S A *114*, E10102–E10111.

Fu, N.Y., Nolan, E., Lindeman, G.J., and Visvader, J.E. (2020). Stem cells and the differentiation hierarchy in mammary gland development. Physiol. Rev. *100*, 489–523.

Gaiko-Shcherbak, A., Fabris, G., Dreissen, G., Merkel, R., Hoffmann, B., and Noetzel, E. (2015). Capturing the differentiation process of MCF10A acini. PLoS One *10*, e0145174.

Goldmann, W.H. (2016). Role of vinculin in cellular mechanotransduction. Cell Biol. Int. *40*, 241–256, Review.

Goldschmidt, M., Peña, L., Rasotto, R., and Zappulli, V. (2011). Classification and grading of canine mammary tumors. Vet. Pathol. *48*, 117–131.

Gudjonsson, T., Rønnov-Jessen, L., Villadsen, R., Rank, F., Bissell, M.J., and Petersen, O.W. (2002). Normal and tumor-derived myoepithelial cells differ in their ability to interact with luminal breast epithelial cells for polarity and basement membrane deposition. J. Cell Sci. *115*, 39–50.

Guelstein, V.I., Tchypysheva, T.A., Ermilova, V.D., and Ljubimov, A.V. (1993). Myoepithelial and basement membrane antigens in benign and malignant human breast tumors. Int. J. Cancer *53*, 269–277.

Haaksma, C.J., Schwartz, R.J., and Tomasek, J.J. (2011). Myoepithelial cell contraction and milk ejection are impaired in mammary glands of mice lacking smooth muscle alpha-actin. Biol. Reprod. *85*, 13–21.

Hilson, J.B., Schnitt, S.J., and Collins, L.C. (2009). Phenotypic alterations in ductal carcinoma in situ-associated myoepithelial cells: Biologic and diagnostic implications. Am. J. Surg. Pathol. *33*, 227–232.

Idoux-Gillet, Y., Nassour, M., Lakis, E., Bonini, F., Theillet, C., Du Manoir, S., and Savagner, P. (2018). Slug/Pcad pathway controls epithelial cell dynamics in mammary gland and breast carcinoma. Oncogene *37*, 578–588.

Iyer, S.V., Dange, P.P., Alam, H., Sawant, S.S., Ingle, A.D., Borges, A.M., Shirsat, N.V., Dalal, S.N., and Vaidya, M.M. (2013). Understanding the role of keratins 8 and 18 in neoplastic potential of breast cancer derived cell lines. PLoS One *8*, e53532.

Jiang, Z., Deng, T., Jones, R., Li, H., Herschkowitz, J.I., Liu, J.C., Weigman, V.J., Tsao, M.S., Lane, T.F., Perou, C.M., and Zacksenhaus, E. (2010). Rb deletion in mouse mammary progenitors induces luminal-B or basal-like/EMT tumor subtypes depending on p53 status. J. Clin. Invest. *120*, 3296–3309.

Jiu, Y., Peränen, J., Schaible, N., Cheng, F., Eriksson, J.E., Krishnan, R., and Lappalainen, P. (2017). Vimentin intermediate filaments control actin stress fiber assembly through GEF-H1 and RhoA. J. Cell Sci. *130*, 892–902.

Jones, J.L., Shaw, J.A., Pringle, J.H., and Walker, R.A. (2003). Primary breast myoepithelial cells exert an invasion-suppressor effect on breast cancer cells via paracrine down-regulation of MMP expression in fibroblasts and tumour cells. J. Pathol. *201*, 562–572.

Kalof, A.N., Tam, D., Beatty, B., and Cooper, K. (2004). Immunostaining patterns of myoepithelial cells in breast lesions: a comparison of CD10 and smooth muscle myosin heavy chain. J. Clin. Pathol. *57*, 625–629.

Klopfleisch, R., von Euler, H., Sarli, G., Pinho, S.S., Gärtner, F., and Gruber, A.D. (2011). Molecular carcinogenesis of canine mammary tumors: News from an old disease. Vet. Pathol. *48*, 98–116, Review.

Krause, S., Maricel, V., Maffini, A., Soto, M., and Sonnenschein, K. (2008). A novel 3D in vitro culture model to study stromal-epithelial interactions in the mammary gland. Tissue Eng.Part C Methods *14*, 261–271.

Lee, C.-H., Kim, M.-S., Chung, B.M., Leahy, D.J., and Coulombe, P.A. (2012). Structural basis for heteromeric assembly and perinuclear organization of keratin filaments. Nat. Struct. Mol. Biol. *19*, 707–715.

Liu, S., Cong, Y., Wang, D., Sun, Y., Deng, L., Liu, Y., Martin-Trevino, R., Shang, L., McDermott, S.P., Landis, M.D., et al. (2014). Breast cancer stem cells transition between epithelial and mesenchymal states reflective of their normal counterparts. Stem Cell Reports *2*, 78–91.

Maxwell, A.J., Clements, K., Hilton, B., Dodwell, D.J., Evans, A., Kearins, O., Pinder, S.E., Thomas, J., Wallis, M.G., and Thompson, A.M.; Sloane Project Steering Group (2018). Risk factors for the development of invasive cancer in unresected ductal carcinoma in situ. Eur. J. Surg. Oncol. *44*, 429–435.

Miller, D.H., Jin, D.X., Sokol, E.S., Cabrera, J.R., Superville, D.A., Gorelov, R.A., Kuperwasser, C., and Gupta, P.B. (2018). BCL11B Drives human mammary stem cell self-renewal in vitro by inhibiting basal differentiation. Stem Cell Reports *10*, 1131–1145.

Molyneux, G., Geyer, F.C., Magnay, F.-A., McCarthy, A., Kendrick, H., Natrajan, R., MacKay, A., Grigoriadis, A., Tutt, A., Ashworth, A., et al. (2010). BRCA1 basal-like breast cancers originate from luminal epithelial progenitors not from basal stem cells. Cell Stem Cell *7*, 403–417.

Nassour, M., Idoux-Gillet, Y., Selmi, A., Côme, C., Faraldo, M.-L., Deugnier, M.-A., and Savagner, P. (2012). Slug controls stem/progenitor cell growth dynamics during mammary gland morphogenesis. PLoS One *7*, e53498.

Pan, X., Hobbs, R.P., and Coulombe, P.A. (2013). The expanding significance of keratin intermediate filaments in normal and diseased epithelial. Curr.Opin.Cell Biol. *25*, 47–56, Review.

Phillips, S., Prat, A., Sedic, M., Proia, T., Wronski, A., Mazumdar, S., Skibinski, A., Shirley, S.H., Perou, C.M., Gill, G., et al. (2014). Cell-state transitions regulated by SLUG are critical for tissue regeneration and tumor initiation. Stem Cell Reports *2*, 633–647.

Pinto, M., Jacobsen, B., and Horwitz, K. (2011). Immunohistochemical method to study breast cancer cell subpopulations and their growth regulation by hormones in three-dimensional cultures. Front.Endocrinol. *2*, 15.

Polyak, K., and Hu, M. (2005). Do myoepithelial cells hold the key for breast tumor progression? J. Mammary Gland Biol. Neoplasia *10*, 231–247, Review.

Pseftogas, A., Xanthopoulos, K., Poutahidis, T., Ainali, C., Dafou, D., Panteris, E., Kern, J.G., Varelas, X., Hardas, A., Gonidas, C., et al. (2020). The tumor suppressor CYLD inhibits mammary epithelial to mesenchymal transition by the coordinated inhibition of YAP/TAZ and TGFB signaling. Cancers (Basel) *12*, e2047.

Pusztaszeri, M. (2010). Phenotypic alterations in myoepithelial cells of the breast in normal and pathologic conditions. Am. J. Surg. Pathol. *34*, 1886, Letter to editor.

Qu, Y., Han, B., Yu, Y., Yao, W., Bose, S., Karlan, B.Y., Giuliano, A.E., and Cui, X. (2015). Evaluation of MCF10A as a reliable model for normal human mammary epithelial cells. PLoS One *10*, e0131285.

Rasotto, R., Goldschmidt, M.H., Castagnaro, M., Carnier, P., Caliari, D., and Zappulli, V. (2014). The dog as a natural animal model for study of the mammary myoepithelial basal cell lineage and its role in mammary carcinogenesis. J. Comp. Pathol. *151*, 166–180.

Reya, T., Morrison, S.J., Clarke, M.F., and Weissman, I.L. (2001). Stem cells, cancer, and cancer stem cells. Nature *414*, 105–111, Review.

Rivera, P., and von Euler, H. (2011). Molecular biological aspects on canine and human mammary tumors. Vet. Pathol. *48*, 132–146, Review.

Rohilla, M., Bal, A., Singh, G., and Joshi, K. (2015). Phenotypic and functional characterization of ductal carcinoma in situ-associated myoepithelial cells. Clin. Breast Cancer *15*, 335–342.

Rønnov-Jessen, L., Petersen, O.W., and Bissell, M.J. (1996). Cellular changes involved in conversion of normal to malignant breast: importance of the stromal reaction. Physiol. Rev. *76*, 69–125, Review.

Runswick, S.K., O'Hare, M.J., Jones, L., Streuli, C.H., and Garrod, D.R. (2001). Desmosomal adhesion regulates epithelial morphogenesis and cell positioning. Nat. Cell Biol. *3*, 823–830.

Russell, T.D., Jindal, S., Agunbiade, S., Gao, D., Troxell, M., Borges, V.F., and Schedin, P. (2015). Myoepithelial cell differentiation markers in ductal carcinoma in situ progression. Am. J. Pathol. *185*, 3076–3089.

Ryser, M.D., Weaver, D.L., Zhao, F., Worni, M., Grimm, L.J., Gulati, R., Etzioni, R., Hyslop, T., Lee, S.J., and Hwang, E.S. (2019). Cancer outcomes in DCIS patients without locoregional treatment. J. Natl. Cancer Inst. *111*, 952–960.

Sánchez-Céspedes, R., Millán, Y., Guil-Luna, S., Reymundo, C., Espinosa de los Monteros, A., and Martín de las Mulas, J. (2016). Myoepithelial cells in canine mammary tumours. Vet. J. *207*, 45–52, Review.

Sanders, M.E., Schuyler, P.A., Dupont, W.D., and Page, D.L. (2005). The natural history of low-grade ductal carcinoma in situ of the breast in women treated by biopsy only revealed over 30 years of long-term follow-up. Cancer *103*, 2481–2484.

Sanders, M.E., Schuyler, P.A., Simpson, J.F., Page, D.L., and Dupont, W.D. (2015). Continued observation of the natural history of low-grade ductal carcinoma in situ reaffirms proclivity for local recurrence even after more than 30 years of follow-up. Mod.Pathol. *28*, 662–669.

Sanghvi-Shah, R., and Weber, G.F. (2017). Intermediate Filaments at the junction of mechanotransduction, migration, and development. Front. Cell Dev. Biol. *5*, 81.

Sarper, M., Allen, M.D., Gomm, J., Haywood, L., Decock, J., Thirkettle, S., Ustaoglu, A., Sarker, S.-J., Marshall, J., Edwards, D.R., and Jones, J.L. (2017). Loss of MMP-8 in ductal carcinoma in situ (DCIS)-associated myoepithelial cells contributes to tumour promotion through altered adhesive and proteolytic function. Breast Cancer Res. *19*, 33.

Sarrio, D., Franklin, C.K., Mackay, A., Reis-Filho, J.S., and Isacke, C.M. (2012). Epithelial and mesenchymal subpopulations within normal basal breast cell lines exhibit distinct stem cell/progenitor properties. Stem Cells *30*, 292–303.

Schaller, G., Fuchs, I., Pritze, W., Ebert, A., Herbst, H., Pantel, K., Weitzel, H., and Lengyel, E. (1996). Elevated keratin 18 protein expression indicates a favorable prognosis in patients with breast cancer. Clin. Cancer Res. *2*, 1879–1885.

Schnitt, S.J., Ellis, I.O., van de Vijver, M.J., Sgroi, D., Lakhani, S.R., Simpson, J., Allred, C., and Vincent-Salomon, A. (2012). Intraductal proliferative lesions: Introduction and overview. In WHO Classification of Tumours of the Breast, 4thEdition, S.R. Lakhani, I.O. Ellis, S.J. Schnitt, P.H. Tan, and M.J. van de Vijver, eds. (IARC), pp. 82–83.

Sirka, O.K., Shamir, E.R., and Ewald, A.J. (2018). Myoepithelial cells are a dynamic barrier to epithelial dissemination. J. Cell Biol. *217*, 3368–3381.

Sleeman, K.E., Kendrick, H., Ashworth, A., Isacke, C.M., and Smalley, M.J. (2006). CD24 staining of mouse mammary gland cells defines luminal epithelial, myoepithelial/basal and non-epithelial cells. Breast Cancer Res. *8*, R7.

Sokol, E.S., Sanduja, S., Jin, D.X., Miller, D.H., Mathis, R.A., and Gupta, P.B. (2015). Perturbation-expression analysis identifies RUNX1 as a regulator of human mammary stem cell differentiation. PLoS Comput. Biol. *11*, e1004161.

Sorenmo, K.U., Rasotto, R., Zappulli, V., and Goldschmidt, M.H. (2011). Development, anatomy, histology, lymphatic drainage, clinical features, and cell differentiation markers of canine mammary gland neoplasms. Vet. Pathol. *48*, 85–97, Review.

Stingl, J., Eaves, C., Zandieh, I., and Emerman, J. (2001). Characterization of bipotent mammary epithelial progenitor cells in normal adult human breast tissue. Breast Cancer Res. Treat. *67*, 93–109.

Uttagomol, J., Ahmad, U.S., Rehman, A., Huang, Y., Laly, A.C., Kang, A., Soetaert, J., Chance, R., The, M.T., Connelly, J.T., and Wan, H. (2019). Evidence for the desmosomal cadherin desmoglein-3 in regulating YAP and Phospho-YAP in keratinocyte responses to mechanical forces. Int. J. Mol. Sci. *20*, pii: E6221.

Uva, P., Aurisicchio, L., Watters, J., Loboda, A., Kulkarni, A., Castle, J., Palombo, F., Viti, V., Mesiti, G., Zappulli, V., et al. (2009). Comparative expression pathway analysis of human and canine mammary tumors. BMC Genomics *10*, 135.

Van Keymeulen, A., Rocha, A.S., Ousset, M., Beck, B., Bouvencourt, G., Rock, J., Sharma, N., Dekoninck, S., and Blanpain, C. (2011). Distinct stem cells contribute to mammary gland development and maintenance. Nature *479*, 189–193.

Vieira, A.F., Ribeiro, A.S., Dionísio, M.R., Sousa, B., Nobre, A.R., Albergaria, A., Santiago-Gómez, A., Mendes, N., Gerhard, R., Schmitt, F., et al. (2014). P-cadherin signals through the laminin receptor α6β4 integrin to induce stem cell and invasive properties in basal-like breast cancer cells. Oncotarget *5*, 679–692.

Vielmuth, F., Wanuske, M.-T., Radeva, M.Y., Hiermaier, M., Kugelmann, D., Walter, E., Buechau, F., Magin, T.M., Waschke, J., and Spindler, V. (2018). Keratins regulate the adhesive properties of desmosomal cadherins through signaling. J. Invest. Dermatol. *138*, 121–131.

Villadsen, R., Fridriksdottir, A.J., Rønnov-Jessen, L., Gudjonsson, T., Rank, F., LaBarge, M.A., Bissell, M.J., and Petersen, O.W. (2007). Evidence for a stem cell hierarchy in the adult human breast. J. Cell Biol. *177*, 87–101.

Weng, Y.-R., Cui, Y., and Fang, J.-Y. (2012). Biological functions of cytokeratin 18 in cancer. Mol. Cancer Res. *10*, 485–493, Review.

Werling, R.W., Hwang, H., Yaziji, H., and Gown, A.M. (2003). Immunohistochemical distinction of invasive from noninvasive breast lesions: a comparative study of p63 versus calponin and smooth muscle myosin heavy chain. Am. J. Surg. Pathol. *27*, 82–90.

Wetzels, R.H., Holland, R., van Haelst, U.J., Lane, E.B., Leigh, I.M., and Ramaekers, F.C. (1989). Detection of basement membrane components and basal cell keratin 14 in noninvasive and invasive carcinomas of the breast. Am. J. Pathol. *134*, 571–579.

Yeong, J., Thike, A.A., Tan, P.H., and Iqbal, J. (2017). Identifying progression predictors of breast ductal carcinoma in situ. J. Clin. Pathol. *70*, 102–108, Review.

Zhang, R.R., Man, Y.-G., Vang, R., Saenger, J.S., Barner, R., Wheeler, D.T., Liang, C.Y., Vinh, T.N., and Bratthauer, G.L. (2003). A subset of morphologically distinct mammary myoepithelial cells lacks corresponding immunophenotypic markers. Breast Cancer Res. *5*, R151–R156.

**iScience, Volume *24***

## Supplemental information

# Cytokeratin 5 determines maturation of the mammary myoepithelium

**Vivi Deckwirth, Eeva Kaisa Rajakylä, Sandhanakrishnan Cattavarayane, Anna Acheva, Niccole Schaible, Ramaswamy Krishnan, Juan José Valle-Delgado, Monika Österberg, Pia Björkenheim, Antti Sukura, and Sari Tojkander**

# SUPPLEMENTAL INFORMATION (SI)

## TRANSPARENT METHODS

### Histological samples of canine mammary tissues

Formalin-fixed paraffin-embedded tissue samples of female canine mastectomy cases (n = 7) with non-infiltrative intraductal proliferative lesions were retrieved from the pathologic-diagnostic archive (Section of Veterinary Pathology, University of Helsinki). Normal mammary gland from the same individual was prerequisite. Respective epidemiological data such as breed, sexual status and age at diagnosis were collected (Fig. S2A).

Histomorphology was reviewed from 4 µm thick hematoxylin and eosin stained tissue sections. Classification criteria of woman for usual ductal hyperplasia (UDH), atypical ductal hyperplasia (ADH) and ductal carcinoma in situ (DCIS) were adopted for canine female non-infiltrative intraductal proliferative lesions (The Consensus Conference Committee, 1997; Collins et al., 2012; Ferreira et al., 2012; Goldschmidt et al., 2011; Mouser et al., 2010; Schnitt et al., 2012b; Simpson et al., 2012). Canine lesions classified as ductal displayed E-cadherin positivity, and invasion was determined as absence of myoepithelial cells and/or extension through the basement membrane (Chocteau et al., 2019; Goldschmidt et al., 2011; Ressel et al., 2011; The Consensus Conference Committee, 1997). Canine UDH applied to intraductal proliferation of small epithelial cells with hyperchromatic nuclei, scant cytoplasm and little nuclear or cellular pleomorphism. Subcategorization as mild, moderate or florid based on the amount of hyperplastic cells forming epithelial bridges and irregular fenestrations filling the ductal lumen. The intraluminal cells displayed positivity for low and/or high molecular weight cytokeratins. Lesions with increased cellular atypia corresponding to low-grade DCIS, but with only partial involvement of the ductal lumen and limited extension classified as ADH. DCIS applied to intraductal epithelial proliferations of increasing cellular atypia allowing categorization into low, intermediate and high nuclear grade DCIS.

### Tissue section immunohistochemistry

Formalin-fixed paraffin-embedded female canine mammary tissue samples were prepared into 4 µm thick serial sections on Menzel Superfrost Plus Adhesion microscope slides (Cat. J1800AMNZ, Thermo Fisher Scientific) and baked at 37 °C o/n. The slides were deparaffinized and rehydrated automated (Leica AutoStainer XL, Leica Biosystems) in xylen and alcohol series before antigen retrieval in a PT Module (LabVision UK Ltd) for 20 min at 99 °C in prewarmed 0.01 M citrate buffer (pH 6.0). After cooling down to RT, the slides were blocked 10 min with 3% hydrogen peroxide in PBS, and rinsed twice with TBS + Tween (Cat. P1379, Sigma). For staining, the BrightVision Poly-HRP-Anti Ms/Rb/Rt IgG Kit (Cat. DPVO110HRP, Immunologic) was used at RT with minor

modifications to manufacturers protocol. Primary mouse antibodies were incubated 1 h at RT and include anti-CK5 (Clone XM26, Cat. 17130, Abcam, dilution 1:75), anti-CK14 (Clone LL002, Cat. 7800, Abcam, dilution 1:300), anti-CK18 (Clone Ks18.04, Cat. 61028, Progen, dilution 1:300), anti-α-SMA (Clone 1A4, Cat. M0851, Dako, dilution 1:600) and primary rabbit anti-E-cadherin (Clone 24E10, Cat. 3195, Cell Signaling Technology, dilution 1:500). For visualization, 3.3´-diaminobenzidine-tetrahydrochloride (Cat. VWRKBS04-110, Immunologic) was applied for 5 min. Harris Hematoxylin (Cat. HX57998853, Merck) was used for 10 sec to counterstain. The slides were dehydrated and mounted with Pertex (Cat. 00811, Histolab). To ensure equal preparation and staining conditions for all the tissue slides, the protocol was implemented on as one batch in one same run. Adjacent normal tissue was internal positive control. From negative controls the antibody was omitted and antibody diluent only was used. Stainings were performed twice.

**Determination of cellular DAB chromogen precipitate intensity**

For determination of color-intensity of basal myoepithelial cytoplasmic 3.3´-diaminobenzidine-tetrahydrochloride chromogen precipitate (i.e. DAB staining intensity, DABi), digital images were generated from IHC stained (α-SMA, CK5 and CK14) female canine mammary tissue slides using a Pannoramic 250 FLASH II digital whole-slide scanner (3DHISTECH Ltd., Budapest, Hungary) with a VCC-FC60FR19CL camera (CIS Corporation, Japan) and LS-6 pulsed Xenon light source (Excelitas Technologies Corp., Waltham, MA, USA). Extended focus was applied with the following settings: Focus distance field of views: 8; Focus levels: 7; Step size (0.2 µm): 5. Resolution of the scanner was 0.24 µm/pixel with a 20x/NA 0.8 objective. To ensure subjection to same imaging conditions, tissue slides were scanned as one batch. For analysis, representative areas of the features (normal, UDH, ADH, DCIS) from each case were imaged at 69.12x magnification using the Pannoramic Viewer Software version 1.15.4 (3DHISTECH Ltd., Budapest, Hungary).

Using Fiji ImageJ Software version 1.51 (U. S. National Institutes of Health, Bethesda, Maryland, USA) the blue wavelength band was separated from TIFF (Tagged Image File Format) image and inverted to 8-bit resolution grey-scale image with intensity values ranging from 0 = black to 255 = white. DABi was determined from individual basal/myoepithelial cells by freehand drawing the boundary of each individual cellular cytoplasmic area (i.e. region of interest, ROI) to be quantified. Inclusion criteria for cells to be analyzed included basal location between the basement membrane and the luminal epithelial cell layer as well as the presence of a nucleus. Manual work allowed precision excluding from the analysis such features as cellular nuclei, overlapping cells and cellular areas showing only cytoplasm without nuclei as well as other positive reactions for the given antibody

(e.g. for α-SMA adjacent myofibroblasts and blood vessels) which would otherwise interfere with the results. DABi was collected as integrated density value, being the product of ROI area and mean pixel value. Mean pixel value is determined as the sum of the grey values of all the pixels in the ROI divided by the number of pixels. DABi values from the intralobular terminal ductal and the extralobular terminal ductal/interlobular ductal segments were collected and analyzed as distinct entities according to their anatomical and physiological differences (Rønnov-Jessen et al., 1996). The used protocol is summarized in Fig. S3B.

**Isolation of canine mammary primary organoids**

Canine normal mammary tissue samples (c. 5 x 10 mm) were collected aseptically into DMEM/F12 medium (Cat. 31330-038, Gibco) from removed tissue (sterilized female, 9 years-of-age, mixed breed of Belgian Sheepdog and German Shepherd Dog) at canine mammary gland surgery (Veterinary Teaching Hospital, University of Helsinki), and kept at 4 °C until macrodissection to remove adherent fat and surplus stroma (LaBarge et al., 2013). The medium was supplemented with 0.25 µg/ml Amphotericin B (Cat. A2942, Sigma), 100 U/ml Penicillin and 100 µg/ml Streptomycin (Cat. 15140-122, Gibco) as well as 10% FBS (Cat. 10500-064, Gibco). Mammary tissue next to the area of sample origin was collected simultaneously into 10% neutral-buffered formalin to confirm histomorphology. After macrodissection, the remaining tissue was cut into 3-4 mm slices for digestion in pre-warmed (37 °C) DMEM/F12 medium supplemented with antibiotica and FBS (as above), 10 µg/ml Insulin (Cat. I6634, Sigma), 200 U/ml Collagenase (Cat. C0130, Sigma), and 100 U/ml Hyaluronidase (Cat. H3506, Sigma) with o/n incubation in a 37 °C water bath using gentle agitation. Digestion was monitored by microscopy using a camera (Canon EOS 600D) attached to an inverted microscope (Olympus CKX41).

Digested material was centrifuged at 600 x g 5 min to separate remaining fat etc. (LaBarge et al., 2013). A 40 µm cell strainer was used to collect the size-differentiated organoid fractions. Media supplemented with antibiotics and FBS (as stated above) was applied for rinsing. The collected material was pelleted at 80 x g 30 s and aliquoted into freezing medium of 50% DMEM/F12 plus 44% FBS plus 6% DMSO (Cat. D2650, Sigma) (StemCell Technologies, 2012) and stored at -130 °C until fluorescence-activated cell sorting (FACS).

**Fluorescence activated cell sorting of canine mammary epithelial cells**

For FACS, the canine organoid fractions were incubated at 37 °C in a humidified 5% $CO_2$ cultivator in DMEM/F12 supplemented with antibiotica and FBS (as stated above), 15.0 µg/ml Insulin (Cat.

I6634, Sigma), 10.0 ng/ml EGF (Cat. E9644, Sigma) and 0.6 µg/ml Hydrocortisone (Cat. H0888, Sigma) for 2-3 d. Differential trypsinization to remove fibroblasts was applied prior generating single-cell suspension for FACS (LaBarge et al., 2013). Single cell suspension of $1x10^6$ cells/ml was generated into HBSS + 1% BSA from canine primary culture using incubation with TrypLE Express (Cat. 12604-013, Gibco) and DNase I (Cat. 11284932001, Roche). Cells were incubated with anti-CD24-Alexa Fluor 405 (Clone ML5, Cat. NB100-77903AF405, Novus Biotechne, 0.7mg/ml) at 4 °C for 45 min in the dark and washed with HBSS + 1% BSA three times. After the last wash, the cells were re-suspended into 500 µl FACS-buffer consisting of PBS + 0.5% BSA followed with a 10 min incubation with a live/dead discriminating stain (Cat. L34975, Invitrogen/Thermo Fisher Scientific). A FACSAria II (BD Biosciences) instrument was used to sort the cells with red (633 nm) and violet (405 nm) lasers at sheat pressure 45.00 and with a 85 µm nozzle. The data was collected using the FACSDiva Software version 8.0.2 (BD Biosciences). Dead cells, non-single cells and $CD24^{neg}$ cells were excluded. The cells were isolated into growth medium (as stated above) in tubes coated by incubation with HBSS + 3% BSA for 2 h under UV-radiation at RT. To determine the sorting purity, the isolated cell population was stained for immunofluorescence imaging prior downstream assay (Fig. S2F). FACS data was analyzed and the graphs generated with the FlowJo Software version 10.4.1 (BD Biosciences).

**Cell culture and siRNA transfections**

Human breast epithelial cell line MCF10A cells (ATCC) were maintained in DMEM/F12 media supplemented with 5% Horse Serum (Cat. 26050088, Gibco), 20 ng/ml EGF (Cat. E9644, Sigma), 0.5 mg/ml Hydrocortisone (Cat. H0888, Sigma), 100 ng/ml Cholera toxin (Cat. C8052, Sigma), 10 µg/ml Insulin (Cat. I6634, Sigma) and 100 U/ml Penicillin and 100 µg/ml Streptomycin (Cat. 15140-122, Gibco). Cells were cultured in an incubator with 5% $CO_2$ at 37 °C.

For siRNA transfections in 2D, MCF10A cells were plated on 35 mm dishes at a density of 5000 cells per well. The following day, cells were transfected with 50 nmol siRNA (human CK5: ON-TARGETplus KRT5 SMART pool siRNA [L-011067-00-0005]; human CK14: ON-TARGETplus KRT14 SMART pool siRNA [L-010602-00-0005]; and human SMA: ON-TARGETplus ACTA2 SMART pool siRNA [L-003450-00-0005]; negative control: ON-TARGETplus Non-targeting siRNA [D-001810-01-05] from Dharmacon) using Ribojuice siRNA transfection reagent (Cat. 71115-3, Millipore) according to the manufacturer´s instructions. On day 4., cells were processed for Western blotting or microscopy. Canine primary cell transfections in 2D conditions were performed as with human MCF10A cells. For canine cells, pool of custom-made siRNAs were used: canine CK5: 5’ UAACUCUUGAAACUCUUCCUU 3’, 5’ AACUCUUGAAACUCUUCCGUU 3’, 5’

ACUCUUGAAACUCUUCCGGUU 3'; canine CK14: 5' UAGUCCUUGGUCUCAGCGGUU 3', 5' UCUCAGAGCGUUCAUUUCCUU 3', UCCACGUUGACAUCUCCGCUU 3'; canine ACTA2 5' UACUUCAAGGUCAGGAUCCUU 3', 5' UCUAUCGGGUACUUCAAGGUU 3', 5' AUGAUGCCGUGUUCUAUCGUU 3' (Dharmacon). In 3D Matrigel cultures of human and canine mammary epithelial cells, siRNAs (50 nmol) were applied after formation of mammospheres (day 5) and incubated for 2 weeks. siRNAs were added to cells every 4 days.

**Fluorescence cell sorting of MCF10A cells**

The FACS protocol from Abcam was followed in this experiment. Briefly, the cells were harvested by trypsinization. Disassociated cells were resuspended at a concentration of approximately $1x10^6$ cells/ml in ice cold PBS, 10% FCS, 1% sodium azide. The cells were fc blocked using Human Fc block (Cat. 564219, BD Biosciences) following manufacturer's instructions. To remove unbound fc block, the cells were washed 3 times by centrifugation at 400 g for 5 min and resuspended in ice cold PBS. 5 µg/ml of the primary antibodies anti-CD49f-FITC (Clone GoH3, Cat. 561893, BD Biosciences) and anti-EpCAM-APC/Cy7 (Clone G8.8, Cat. 118217, Biolegend) were added to the cells and incubated for 1 h at 4°C in the dark. The cells were washed as described in the previous steps and resuspended in ice cold PBS, 10% FCS, 1% sodium azide. The cell suspension was immediately stored at 4°C in the dark. The cells were sorted using a FACSAria II (BD Biosciences) instrument at sheat pressure 45.00 with a 85 µm nozzle and the blue (488 nm) as well as red (633 nm) lasers. The flow cytometer settings adjustments and subsequent data collection was done using FACSDiva Software version 6.1.3 (BD Biosciences). Compensation was performed using unstained cells and single stained control cells. The data generated was analyzed using FlowJo Software version 10.6.1.

**Lentiviral-based RNA interference**

Lentiviral RNA interference was done as described in Cattavarayane et al., 2015. The packaging vector containing the desired shRNA construct was received from SIGMA. The helper plasmids pMD2.G (Plasmid 12259), and pMDL g/p RRE (Plasmid 12251) and pRSV-Rev (Plasmid 12253) were provided by Addgene. DNA transfections were performed by using Lipofectamine 2000 (Invitrogen). The packaging vector: pVSVG : pMDL g/p RRE : pRSV-Rev were used in 3:1:1:1 proportion and the total DNA used for transfection was 20 µg (15µg :: 2.5 µg : 830 ng : 830 ng : 830 ng). Nearly confluent (70–80%) 293 T cells were grown on Corning CellBind (Cat. 3296) 6 well plate for transfections. 24 hrs post transfection, media containing the transfection mix was removed carefully and 1 ml of fresh media was added. The media supernatant containing the viral particles

was collected every 12 hrs for 3–4 days and stored at 4 °C. The viral supernatants were pooled and centrifuged at 1000 rpm for 5 minutes and filtered through a 0.44 µm filter. The cells were infected using viral supernatant for 24 hrs in the presence of 4 µg/ml polybrene (Cat. 107689, Sigma) and the infected cells were selected using puromycin (4 µg/ml, Sigma). The puromycin selected cells were expanded and stored by freezing in 90% FCS, 10% DMSO (Sigma) at -130 °C.

**Western blotting**

Cells were washed with PBS and lysed in 1% Triton X-100/PBS, containing protease and phosphatase inhibitors (Cat. 539131 and Cat. 539131, Calbiochem). Protein concentrations were measured with Qubit® Protein Assay Kit (ThermoFisher Scientific). Sample loading buffer, 4x LSB-DTT, was added to lysates and samples were boiled for 5´ before loading in SDS-PAGE gels (Bio-Rad). Wet transfer (Bio-Rad) with Immobilon-P Membrane, PVDF filter (Millipore) was used for blotting. Mixture of 5% BSA and 5% milk was used for blocking for at least 1 h. Following antibodies were used for detection of specific proteins: mouse anti-CK5 (Clone XM26, Cat. ab17130, Abcam), mouse anti-CK6 (Clone B-7, Cat. sc-514520, Santa Cruz), mouse anti-CK14 (Clone LL002, Cat. ab7800, Abcam), rabbit anti-CK18 (Polyclonal, Cat. ab24561, Abcam), mouse anti-CK19 (Clone BA-17, Cat. ab7755, Abcam), mouse anti-Pan-Keratin (Clone C11, Cat. 4545, Cell Signaling Technology; Recognizing CK4, 5, 6, 8, 10, 13 and 18), mouse anti-SMA (Clone 1A4, Cat. A5228, Sigma), rabbit anti-E-cadherin (Clone 24E10, Cat. 3195, Cell Signaling Technology), rabbit anti-P-Thr18/Ser19-MLCII (Clone Thr18/Ser19, Cat. 3674, Cell Signaling Technology), mouse anti-calponin1 (Clone CALP, Cat. sc-58707, Santa Cruz), rabbit anti-Vimentin (Clone D21H3, Cat. 5741, Cell Signaling Technology), mouse anti-Dsg3 (Clone 5H10, Cat. sc-23912, Santa Cruz), rabbit anti-P-cadherin (Clone C13F9, Cat. 2189, Cell Signaling Technology), rabbit anti-Slug (Clone C19G7, Cat. 9585, Cell Signaling Technology) and mouse anti-GAPDH (Clone GAPDH-71.1, Cat. G8795, Sigma). Anti-mouse or -rabbit HRP-linked secondary antibodies (Cell Signaling Technology) in 1:3000 dilution and Western HRP substrate (Cat. WBLUR0100, Luminata™Crescendo, Millipore) were used for chemiluminescence detection of the protein bands. Images were taken with Fujifilm LAS-3000 Imager using autoexposure-setting that choose the optimal exposure time for each blot.

**Immunofluorescence microscopy**

Cells were cultured on coverslips and washed with PBS prior to fixation with 4% PFA. Permeabilization was performed with 0.1% Triton X-100 in TBS for 5´ and cells on coverslips were moved to 0.2% Dulbecco/BSA. The following primary antibodies were used for stainings in 1:50 dilutions: mouse anti-CK5 (Clone XM26, Cat. ab17130, Abcam), mouse anti-CK14 (Clone LL002,

Cat. ab7800, Abcam), rabbit anti-P-Ser18/Thr19-MLCII (Clone Thr18/Ser19, Cat. 3674S, Cell Signaling Technologies), rabbit anti-E-cadherin (Clone 24E10, Cat. 3195, Cell Signaling Technologies), mouse anti-vinculin (Clone hVin-1, Cat. V9264, Sigma), and mouse anti-Dsg3 (Clone 5H10, Cat. sc-23912, Santa Cruz), mouse anti-Laminin-5 (Clone D4B5, Cat. MAB19562, Sigma-Aldrich). Alexa Fluor α-rabbit 488 and α-mouse 568 (Life TechnologiesTM) secondary antibodies were used to detect the primary antibodies. Actin cytoskeleton was detected with Alexa-488-, -568- and -647-Phalloidins in 1:200 dilution (Life TechnologiesTM) and DNA with DAPI (Life TechnologiesTM). DABCO/Mowiol was used for mounting. Images were acquired with Leica DM6000 and Leica DM5000 upright fluorescence wide field microscopes equipped with a Hamamatsu Orca-Flash4.0 V2 sCMOS camera.

**3D mammosphere cultures**

Matrigel, ECM gel from Engelbreth-Holm-Swarm murine sarcoma (Sigma E1270) was prepared according to manufacturer's instructions. MCF10A cells were trypsinized and approximately 5000 cells in F12 media were seeded on top of the Matrigel-coated eight-chamber slides. Formation and morphology of spheres were monitored frequently under a light microscope. After two weeks, 3D structures were fixed with 2% PFA and diameter of the structures were calculated from bright field images using ImageJ. For IF, cells were permeabilized with 0.25% Triton-X in PBS for 10 min. Unspecific binding sites were blocked with IF buffer (0.1% BSA, 0.2% Triton-X, 0.05% Tween in PBS) supplemented with 10% goat serum at RT for 1 h. Primary antibodies in blocking solution were incubated o/n at 4 °C and secondary antibodies at RT for 30 mins. Cytoskeletal structures were stained with Phalloidin and nucleus with DAPI. Samples were mounted with Mowiol/DABCO. The IF stainings of 3D spheroids were performed as in https://brugge.med.harvard.edu/protocols with minor modifications. Imaging stacks was performed with Leica TCS SP5. Objective used: HCX PL APO 20x/0,7 Imm Corr (water, glycerol, oil) Lbd.bl.

**Determination of cell elastic modulus by atomic force microscopy**

The elastic moduli of MCF10A, CK5 KD, and CK14 KD cells were determined by cell indentation experiments using a MultiMode 8 atomic force microscope (AFM) with a NanoScope V controller and a closed-loop PicoForce scanner (Bruker, Santa Barbara, CA). The cells, grown on coverslips coated with LN111, were mounted in the AFM and indented with triangular MLCT probes (Bruker) with nominal tip radius of 20 nm and spring constants about 0.05 N/m, obtained by the thermal noise method (Hutter and Bechhoefer, 1993). The deflection sensitivity was measured on a hard, freshly

cleaved mica surface just before the experiments with cells. Cell indentation was carried out with the AFM operating in Force Volume mode (contact mode), collecting indentation force curves in 40 × 40 $\mu m^2$ areas, the so-called force maps, which were divided into 16 × 16 pixels. A force curve was recorded at each pixel of the force map (that is, 256 force curves per force map) by indenting the cells at 4 µm/s rate, with maximum applied forces typically in the range of 1.0–1.5 nN. The experiments were carried out in PBS at 37 °C (Thermal Applications Controller, Bruker). The elastic modulus of the cells were obtained by fitting the approach indentation curves with the Sneddon (conical indenter) model (Sneddon, 1965), using the software NanoScope Analysis 1.5 (Bruker). Between 440 and 750 indentation curves from 2 or 3 different 40 × 40 µm2 force maps, corresponding to about 8 to 12 cells, were analyzed for each cell type. The indentation depth was typically in the range 1.5 – 2.5 µm. The corresponding elastic modulus histograms were fit with three Gauss distributions using OriginPro 2020 software.

**Traction force microscopy**

For traction force microscopy experiments in the single cell, the cell doublet, or the monolayers, cells were plated on elastic collagen-1-coated polyacrylamide (PAA) gel substrates with a stiffness (Young's Modulus/elastic modulus) of 4 kPa (single cell) or 6.3 kPa (cell doublet) and incubated for 2-4 h prior to imaging. Gel substrates were surface-coated with sulfate fluorescent microspheres (Invitrogen, diameter 200 nm) before coating with collagen-1. Single cells together with the underlying microspheres were imaged at multiple locations with 3I Marianas imaging setup containing a heated sample chamber (37 °C) and controlled $CO_2$ (3I intelligent Imaging Innovations, Germany). 63x/1.2 W C-Apochromat Corr WD=0.28 M27 objective was used. Following live cell imaging, the cells were detached from the substrates with 10x Trypsin (Lonza Group) and a second set of microsphere images was taken to serve as reference images. Displacement maps for microspheres were achieved by comparing the reference microsphere images to the experimental images and by knowing the cell-induced displacement field, substrate stiffness (4 kPa), and a manual trace of the cell boundary, we computed the cell-exerted traction fields by using Fourier Transform Traction Cytometry (Krishnan et al., 2009; Tolić-Nørrelykke et al., 2002). Root mean squared magnitudes were computed from the traction fields. For the measurement of intercellular stresses, we utilized cell doublets. These assays were performed at 6.3 kPa PAA dishes, with an optical resolution of 63x and analyzed at a spatial resolution of ~1µm.

## Colocalization analyses

Colocalization of actin (Phalloidin) and Dsg3 at cell-cell junctions was analyzed in Fiji. Manually drawn areas of cell-cell junctions were used as regions of interest, ROI, and colocalization (in %) on this region was analyzed with FIJI colocalization analysis.

## Analyses of laminin-5 intensity from 3D spheroids

Raw data images from laminin-5 stainings of 3D mammospheres were imported to Fiji and line profiles, starting immediately outside the spheroid structures, were drawn towards the cell center (Fig. 6A). 3-5 line profiles were drawn around one spheroid. Intensity maps of the stainings were also performed to better demonstrate the differences in between samples. Numerical values from the line profiles were exported to excel. Of these data, the third point from the line profiles mostly displayed highest intensity values within the studied samples and was chosen for further analysis to compare the laminin-5 intensities in between different samples/spheroids. t-test (two-tailed, equal variance) was used to analyse the statistical significance of these peak values in between groups.

## Statistical analysis

Standard deviations and statistically significant difference between means of two groups (t-test) were analyzed in Microsoft Excel 2013. Mann–Whitney–Wilcoxon rank-sum test was performed with Origin 2018. For statistical analysis of DAB chromogen staining intensity (DABi), multilevel mixed linear model was performed using the IBM SPSS Software version 25.0 (IBM Corp., USA). The fixed main effects of age, gender, DABi biomarker group (i.e. CK5, CK14 and α-SMA), ductal segment and pathologic-anatomic diagnosis (PAD) on the DABi-values were examined. The DABi biomarker group, PAD and the interaction between biomarker group and PAD were regarded as fixed effects. Random intercepts for dog individual and ductal segment (i.e. intralobular terminal duct, extralobular terminal duct/interlobular duct) were used to account for the hierarchical structure of the data. Thus, individual basal myoepithelial cells (i.e. observation unit) were nested (clustered) within ductal segments and ductal segments nested within dogs. DABi-values were ln-transformed for the statistical analysis due to skewed distribution. Bonferroni's multiple comparisons correction was used when comparing more than 2 groups, that is DABi biomarker groups and PAD groups within and between ductal segments. Pairwise comparison over all the individual companions was implemented. The level of significant was defined as $p < 0.05$. No statistical methods were used to predetermine the DABi biomarker study sample size.

## SUPPLEMENTARY FIGURES

**A**

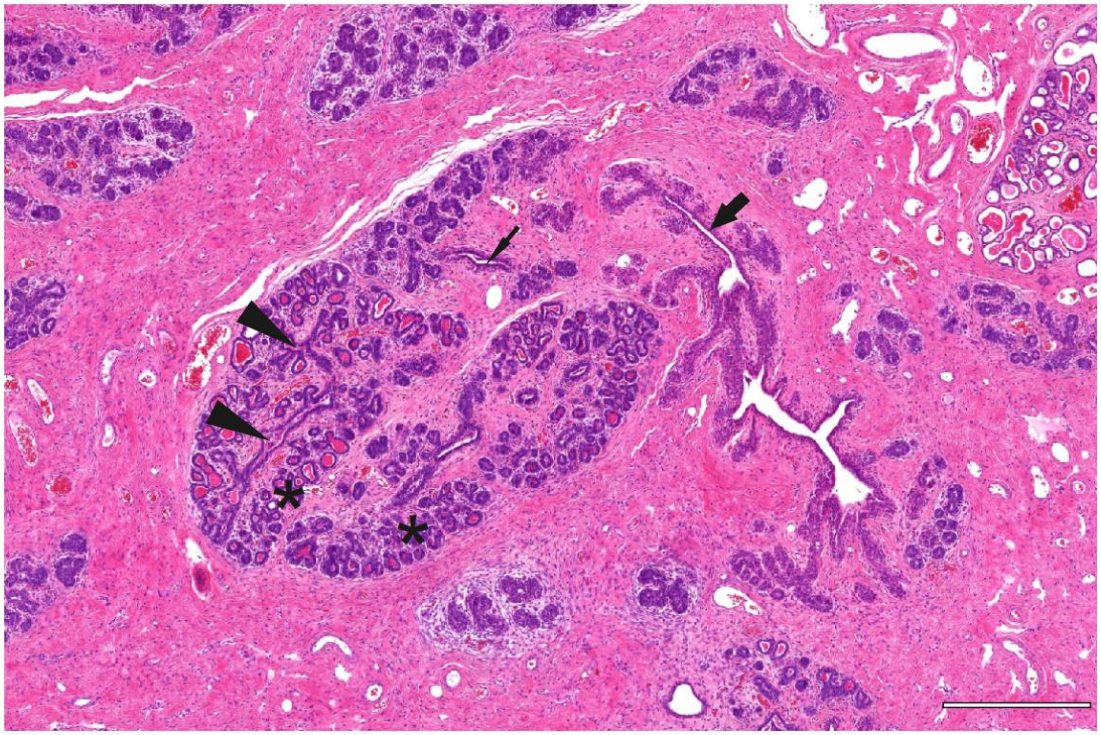

**B**

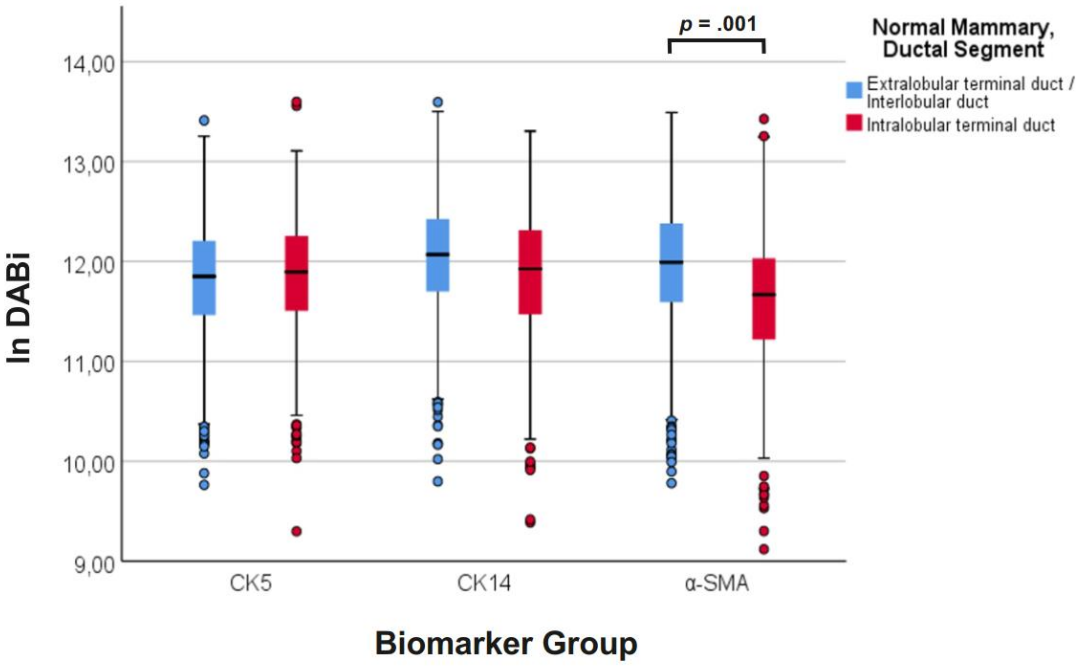

**Figure S1: Expression of basal myoepithelial biomarkers in normal mammary ductal segments, Related to Figure 1. A)** Histomorphology of the canine mammary terminal duct lobular unit (TDLU) consisting of a lobule with acinar units (asterix) and intralobular terminal duct (wedge) as well as extralobular terminal duct (thin arrow), leading into interlobular duct (thick arrow). Hematoxylin and eosin (HE) staining. Bar 500 µm. **B)** Boxplot showing the difference in between the cellular ln-transformed DAB intensity (ln DABi) values for the basal myoepithelial biomarkers CK5, CK14 and α-SMA in between the normal intralobular terminal ductal segment (CK5 n(cells)=612; CK14 n=816; α-SMA n=875) and the extralobular terminal / interlobular ductal segment (CK5 n=1203; CK14 n=1469; α-SMA n=1765). Canine patient n=7. Black middle line within box represents median. Height of box is interquartile range (IQR), representing $75^{th}$ and $25^{th}$ percentiles, respectively. Whiskers represent the lowest and highest data within the 1.5 x IQR of the lower and upper quartiles, respectively. Circles represent outliers. Linear mixed model with random intercepts for canine individual and ductal segment was used with Bonferroni's multiple comparisons correction. The level of significant was defined as $p < 0.05$. Only statistically significant mean differences are indicated. Significant difference was determined between the normal ductal segments in the expression of α-SMA ($p = 0.001$).

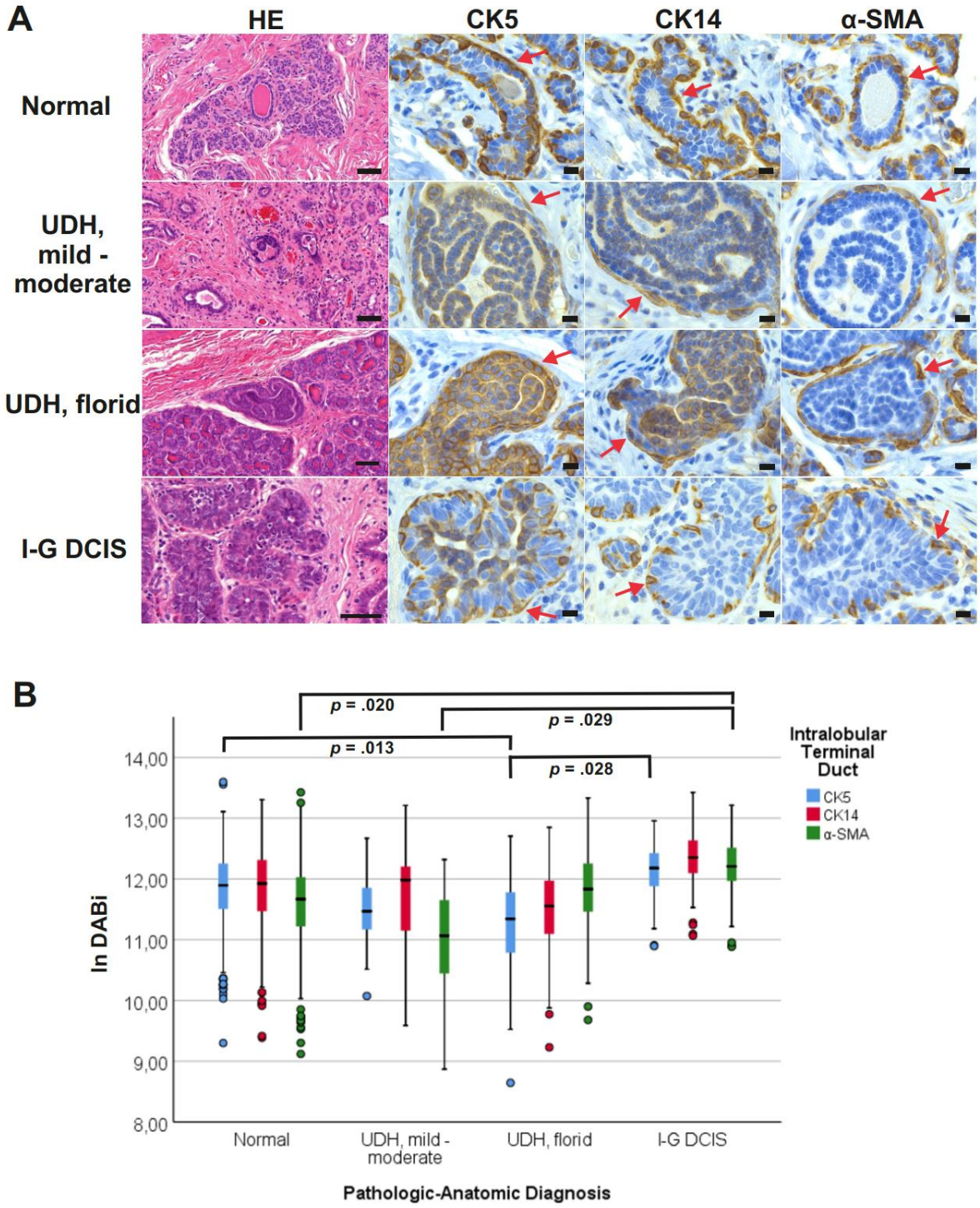


**Figure S2. Expression of CK5, CK14 and α-SMA in the intralobular terminal ductal segment upon intraductal hyperplasia, Related to Figure 1. A)** Consecutive canine mammary FFPE tissue sections of normal, mild-to-moderate usual ductal hyperplasia (UDH, mild-to-moderate), florid usual ductal hyperplasia (UDH, florid) and intermediate-grade ductal carcinoma in situ (I-G DCIS) were stained using hematoxylin-eosin (HE, far left) and the basal myoepithelial markers CK5 (middle left), CK14 (middle right) and α-SMA (far right). Representative images of the lesions are shown. Red

arrows indicate basal myoepithelial layer as distinct from intraluminal cellular hyperplasia. Bar for HE in normal, mild-moderate UDH, florid UDH and I-G DCIS 50 µm, and in all IHC 10 µm. **B)** Boxplot of the quantifications of intralobular terminal ductal cellular ln-transformed DAB intensity (ln DABi) values for normal CK5 n(cells)=612, CK14 n=816, α-SMA n=875; UDH mild-to-moderate CK5 n=22, CK14 n=17, α-SMA n=29, UDH florid CK5 n=151, CK14 n=203, α-SMA n=258; I-G DCIS CK5 n=105, CK14 n=184, α-SMA n=153. Canine patient n=7. Black middle line within box represents median. Height of box is interquartile range (IQR), representing $75^{th}$ and $25^{th}$ percentiles, respectively. Whiskers represent the lowest and highest data within the 1.5 x IQR of the lower and upper quartiles, respectively. Circles represent outliers. Linear mixed model with random intercepts for canine individual and ductal segment was used. Pairwise comparison over all the individual companions was implemented with Bonferroni's multiple comparisons correction. The level of significant was defined as $p < 0.05$. Only statistically significant mean differences are indicated.

A

| Case nr. | Breed | Gender | Age at diagnosis |
|---|---|---|---|
| 1 | Skye Terrier | Intact female | 9 |
| 2 | German Shepherd Dog | Intact female | 7 |
| 3 | Mixed | Sterilized female | 8 |
| 4 | Jack Russel Terrier | Sterilized female | 12 |
| 5 | Bichon Frise | Intact female | 11 |
| 6 | Japanese Spitz | Sterilized female | 6 |
| 7 | Mixed | Intact female | 9 |

B

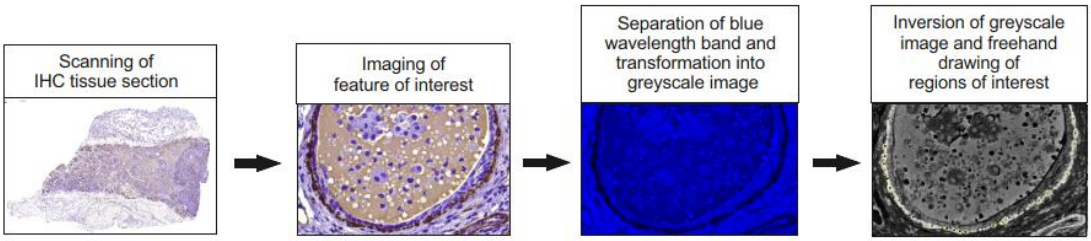


C

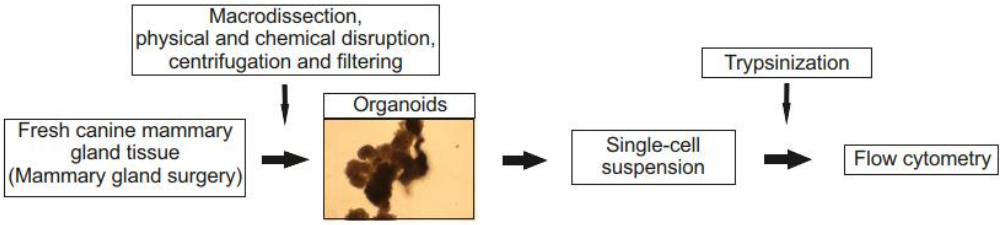


D E

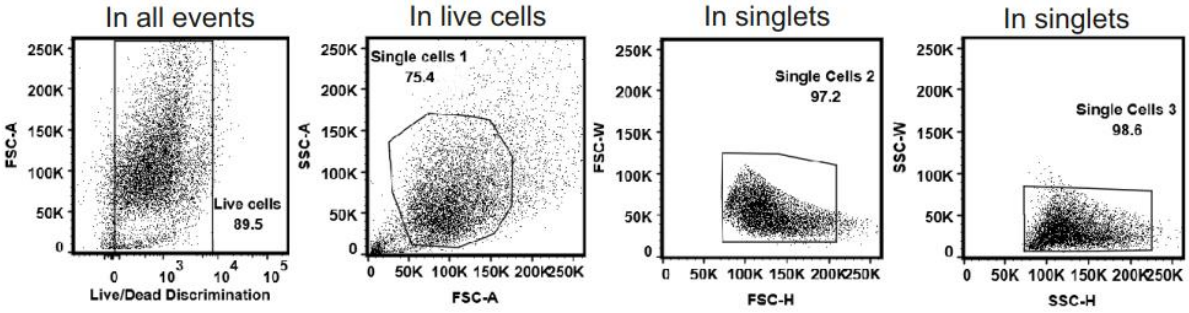


Exclusion of doublets

F

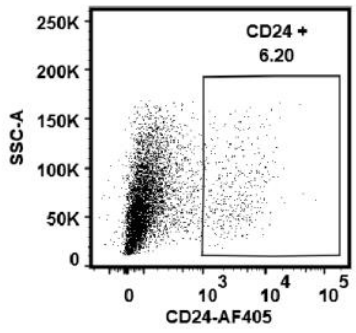


G

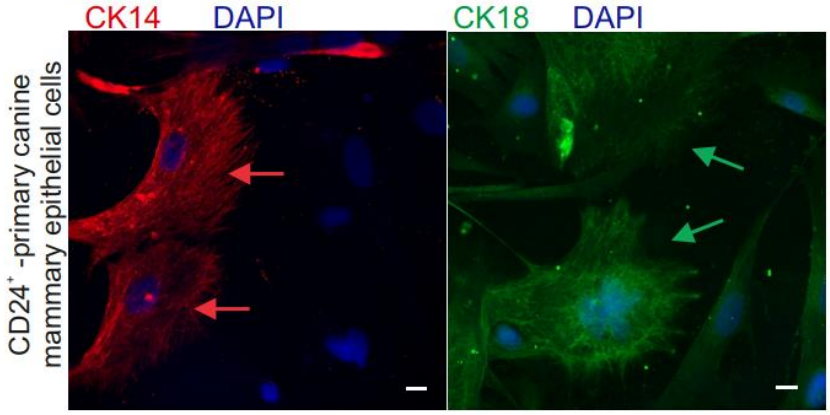

**Figure S3: Determination of DAB intensity and isolation of epithelial cells for siRNA experiments from canine mammary gland, Related to Figure 1 and Figure 2. A)** Patient data of canine cases selected for DAB intensity determination of basal myoepithelial markers α-SMA, CK5 and CK14. **B)** Scheme summarizing the protocol used to determine the DAB intensity (DABi) of basal myoepithelial markers α-SMA, CK5 and CK14 from canine mammary gland tissue sections stained with immunohistochemistry. Tissue section scans were generated with a Pannoramic 250 FLASH II digital scanner and features of interest imaged using Pannoramic Viewer. The 8-bit blue wavelength band image was separated, transformed into greyscale and inverted using ImageJ, followed by determination of the DABi from freehand-drawn cellular regions of interest (yellow in image far right). **C)** Scheme summarizing the protocol used to isolate mammary epithelial cells from freshly collected canine mammary gland tissue. **D-F)** FACS isolation strategy of $CD24^+$ canine mammary epithelial cells showing the proportion of parent cells for each gate. **D)** Single-cellular suspension of canine mammary epithelial cells gated for live cells using LIVE/DEAD® Fixable Near-IR Red. **E)** Doublets and larger cell clumps were discriminated in live cells population. Scatter Gate display (left), FSC Gate display (middle) and SSC Gate display (right). **F)** Single-cells gated by CD24-AF405 for $CD24^+$ population representing epithelial cells. FSC-A = Forward Scatter Area; SSC-A = Side Scatter Area; FSC-W = Forward Scatter Width; FSC-H = Forward Scatter Height; SSC-W = Side Scatter Width; SSC-H = Side Scatter Height. **G)** Immunofluorescence stainings of the $CD24^+$ -primary canine mammary epithelial cells with specific antibodies against CK14 (red) and CK18 (green). Nuclei were stained with DAPI (blue). Bar 10 µm.

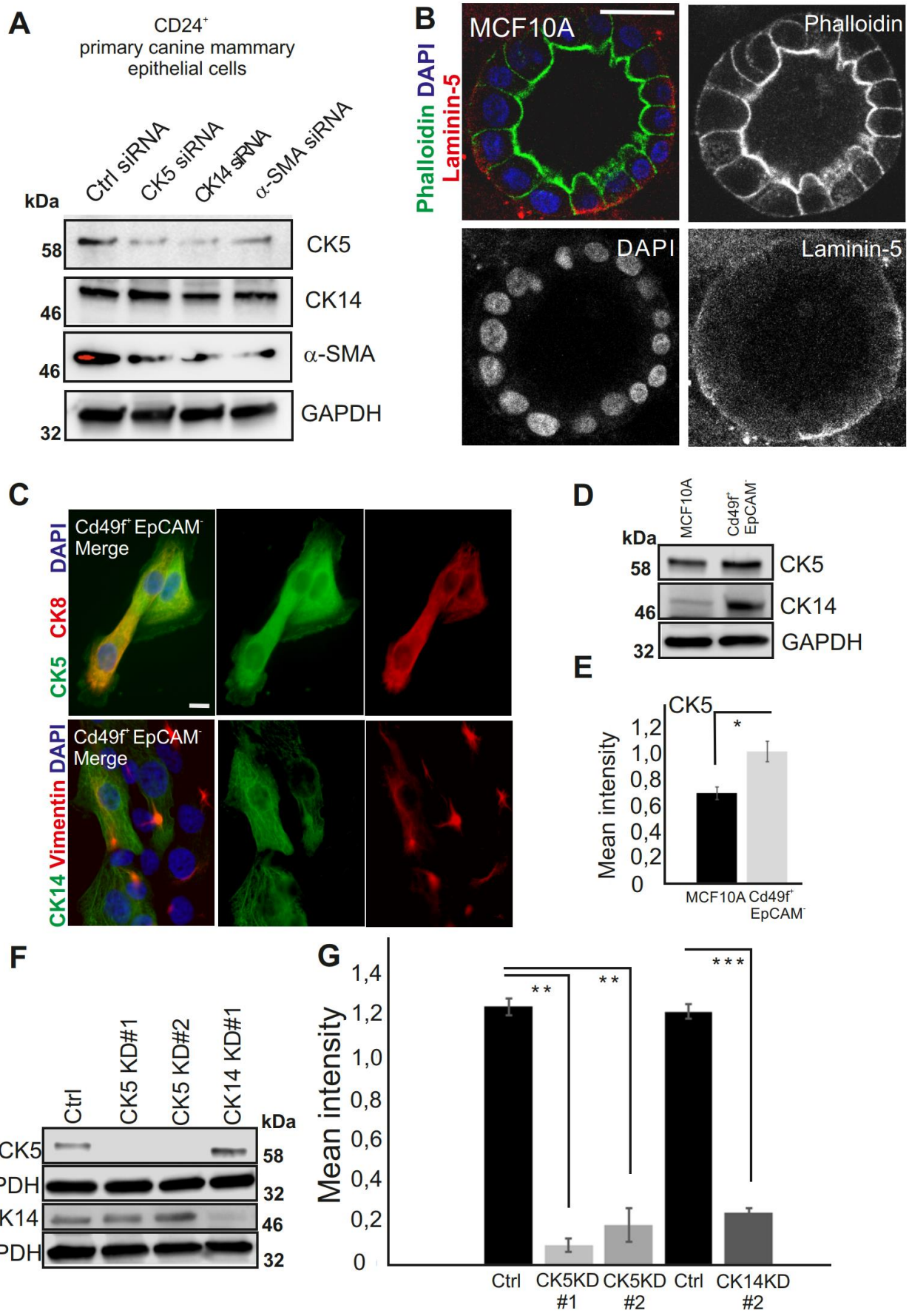
A
CD24+
primary canine mammary
epithelial cells
Ctrl siRNA
CK5 siRNA
CK14 siRNA
α-SMA siRNA
kDa
58
CK5
46
CK14
46
α-SMA
32
GAPDH
B
MCF10A
Phalloidin DAPI
Laminin-5
Phalloidin
DAPI
Laminin-5
C
Cd49f+ EpCAM-
Merge
DAPI
CK8
CK5
Cd49f+ EpCAM-
Merge
CK14 Vimentin DAPI
D
MCF10A
Cd49f+
EpCAM-
kDa
58
CK5
46
CK14
32
GAPDH
E
CK5
Mean intensity
1,2
1,0
0,8
0,6
0,4
0,2
0
*
MCF10A
Cd49f+
EpCAM-
F
Ctrl
CK5 KD#1
CK5 KD#2
CK14 KD#1
kDa
CK5
58
GAPDH
32
CK14
46
GAPDH
32
G
Mean intensity
1,4
1,2
1,0
0,8
0,6
0,4
0,2
0
**
**
***
Ctrl
CK5KD
#1
CK5KD
#2
Ctrl
CK14KD
#2

**Figure S4: Knock-down of α-SMA, CK5 and CK14 from canine and human mammary epithelial cells, Related to Figure 2. A)** Depletion of primary canine mammary epithelial cells ($CD24^+$) by specific siRNAs against CK5, CK14 and α-SMA on 2D cell culture conditions. Cellular lysates were performed 4 days after application of siRNAs and protein levels were assessed in Western blotting by specific antibodies. GAPDH acts as a loading control. **B)** MCF10A cells, cultured for 2 weeks in 3D Matrigel, display hollow lumen and secretion of basement membrane proteins. Specific antibody against laminin-5 was utilized for PFA-fixed spheroids and Phalloidin was used to visualize actin cytoskeleton and DAPI nuclei. Bar 50 um. **C)** FACS-sorted $CD49f^+$ $EpCAM^-$ - mammary epithelial cell population enriched for basal progenitors, isolated from MCF10A cells and stained with specific antibodies against CK5, CK8, CK14 and vimentin. Nuclei were visualized with DAPI. Isolated cells display CK5/CK8 double positive cells and cells displaying either CK14 or vimentin. Bar 20 µm. **D)** Comparison of parental cell line MCF10A and FACS-sorted $CD49f^+$ $EpCAM^-$ cell population. Cellular lysates were utilized in Western blotting to assess the levels of CK5 and CK14. GAPDH acts as a loading control. **E)** Quantification of CK5, related to Figure S3D. Mean (± SEM) is shown; n=3; *P<0.05 (paired t-test)**. F)** Lentiviral-based RNA interference was utilized to deplete CK5 and CK14 from $CD49f^+$ $EpCAM^-$ - mammary epithelial cell population enriched for basal progenitors. Western blotting was used to confirm the efficiency of depletion. GAPDH was used as a loading control. **G)** Quantification of the CK5 and CK14 levels from ctrl ($CD49f^+$ $EpCAM^-$, enriched for basal progenitors), CK5 KD and CK14 KD cells, related to Figure S3F. Mean (± SEM) is shown; n=3; **P<0.01; ***P<0.001 (paired t-test).

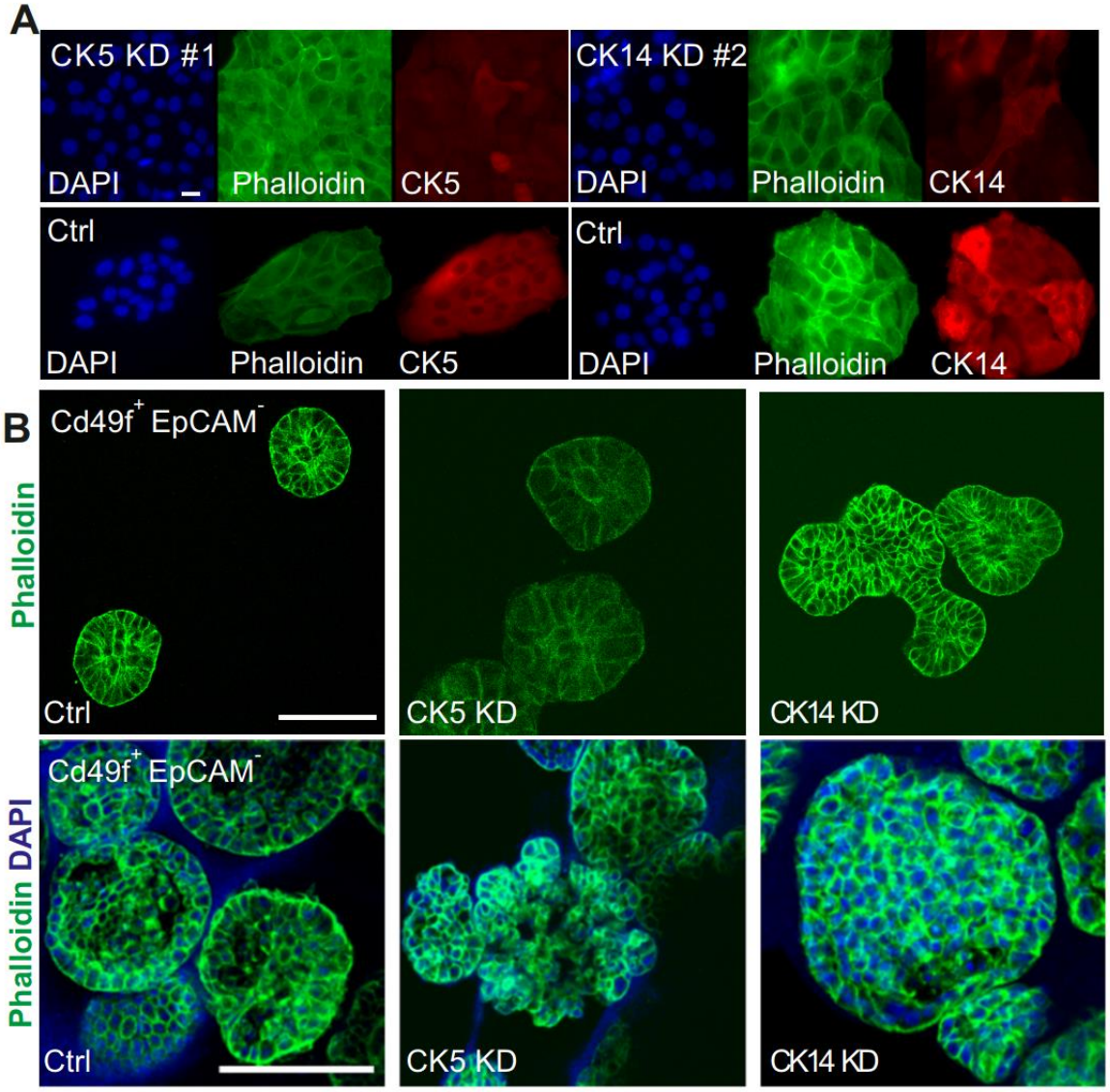
A
CK5 KD #1
DAPI
Phalloidin
CK5
CK14 KD #2
DAPI
Phalloidin
CK14
Ctrl
DAPI
Phalloidin
CK5
Ctrl
DAPI
Phalloidin
CK14
B
Cd49f+ EpCAM-
Phalloidin
Ctrl
CK5 KD
CK14 KD
Cd49f+ EpCAM-
Phalloidin DAPI
Ctrl
CK5 KD
CK14 KD

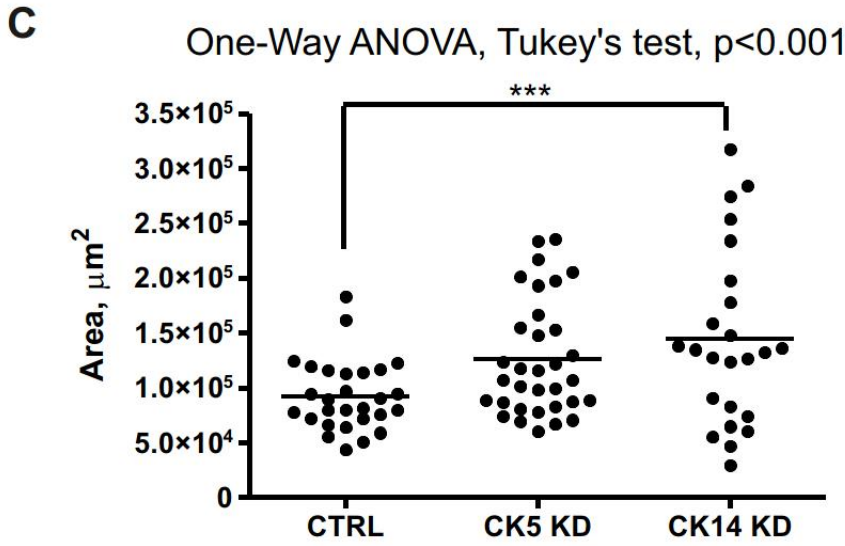
C
One-Way ANOVA, Tukey's test, p<0.001
***
Area, μm2
3.5×10^5
3.0×10^5
2.5×10^5
2.0×10^5
1.5×10^5
1.0×10^5
5.0×10^4
0
CTRL
CK5 KD
CK14 KD

420

421

**Figure S5: Depletion of CK5 and CK14 from CD49f$^{+}$ EpCAM$^{-}$ basal progenitor-enriched MCF10A mammary epithelial cell population, Related to Figure 2. A)** Immunofluorescence stainings of the created knock down cell lines with specific antibodies against CK5 and CK14. Actin cytoskeleton was visualized with Phalloidin and nuclei with DAPI. **B)** Depletion of CK5 and CK14 from 3D cultures of CD49f$^{+}$ EpCAM$^{-}$ basal progenitor-enriched MCF10A mammary epithelial cells. Cultures were maintained for two weeks, after which they were fixed with PFA and stained with Phalloidin (green) and DAPI (blue). Representative immunofluorescence images of two sets of 3D mammospheres from separate experiments are shown. In the upper panel visualized with Phalloidin and lower with Phalloidin and DAPI. Bar 100 μm**. C)** Measurement of spheroids area was performed with Fiji-ImageJ 1.52p (National Institutes of Health, Bethesda, MD, USA, http://imagej.nih.gov/ij/, 1997-2019) software using free-hand selection tool and the built-in area measurement function. ***P<0.001 (One-Way ANOVA analysis, Tukey's post-test.

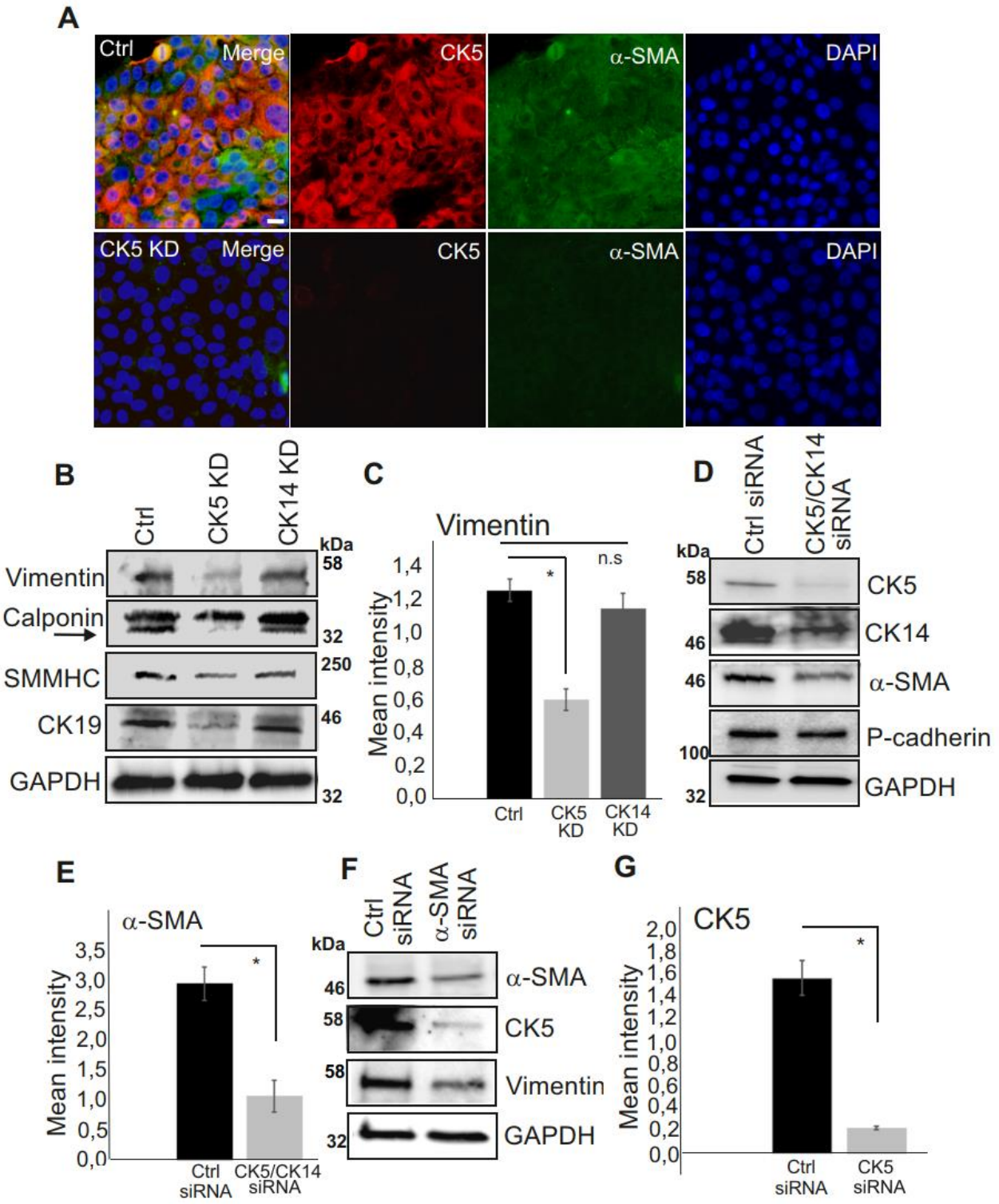


**Figure S6: Depletion of CK5 leads to downregulation of markers for mature myoepithelium, Related to Figure 2 and Figure 3. A)** Immunofluorescence stainings of ctrl ($CD49f^+$ $EpCAM^-$, enriched for basal progenitors) and CK5 KD cells were stained with specific antibodies against CK5 and α-SMA. Nuclei were visualized with DAPI. Bar 20 µm. **B)** Cellular lysates from ctrl ($CD49f^+$

EpCAM$^-$, enriched for basal progenitors), CK5 and CK14 KD cell lines were utilized in Western blotting. Specific antibodies against vimentin, calponin 1, smooth muscle myosin heavy chain (SMMHC) and CK19 were used in blotting. GAPDH was used as a loading control. **C)** Quantification of vimentin levels, related to Fig. S5B. Mean (± SEM) is shown; n=3; *P<0.05 (paired t-test); n.s.= not significant. **D)** Scrambled siRNA and specific siRNAs against CK5 in combination with CK14 siRNA were utilized in MCF10A cells. Cellular lysates were performed four days after incubation and protein levels for CK5, CK14, α-SMA and P-cadherin were detected in Western blotting with specific antibodies. GAPDH acts as a loading control. **E)** Quantification of the α-SMA levels showed significant decrease upon CK5/CK14 depletion. Mean (± SEM) is shown; n=3; *P<0.05 (paired t-test). **F)** Depletion of α-SMA was performed with specific siRNAs in MCF10A cultures for four days. Cellular lysates from control siRNA and α-SMA siRNA- treated cells were used in Western blotting and specific antibodies against α-SMA, CK5 and vimentin were utilized to assess their levels. GAPDH was used as a loading control. Quantification of the CK5 levels showed significant decrease. **G)** Quantification of CK5 levels, related to Figure S5F. Mean (± SEM) is shown; n=3; *P<0.05 (paired t-test).

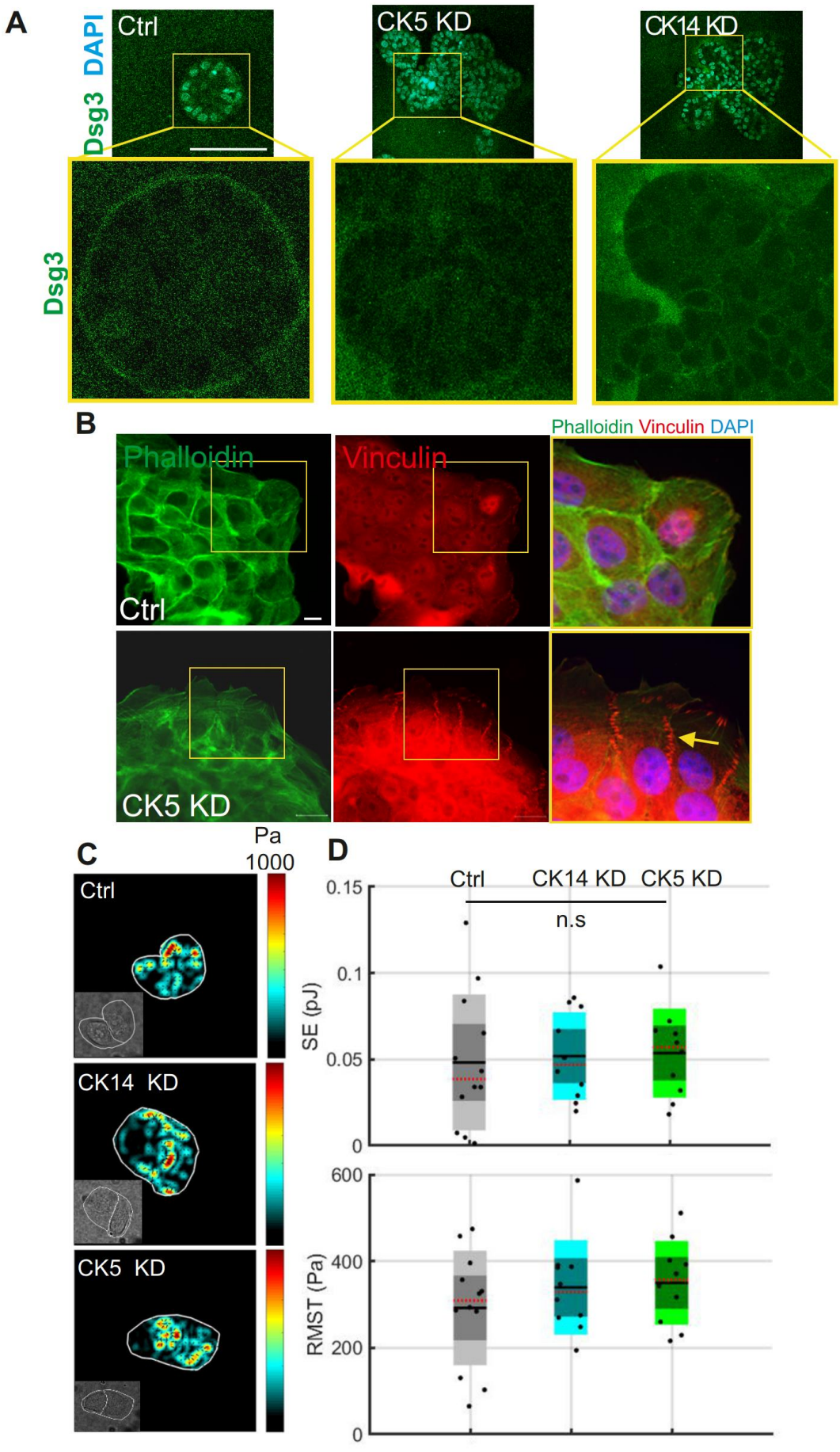
A
Dsg3 DAPI
Ctrl
CK5 KD
CK14 KD
Dsg3
B
Phalloidin
Vinculin
Phalloidin Vinculin DAPI
Ctrl
CK5 KD
C
Pa
1000
Ctrl
CK14 KD
CK5 KD
D
Ctrl
CK14 KD
CK5 KD
n.s
SE (pJ)
0.15
0.1
0.05
0
RMST (Pa)
600
400
200
0

**Figure S7: Knock down of CK5 impacts myoepithelial cell-cell junction proteins, Related to Figure 4 and 5. A)** 3D cultures of $CD49f^{+}$ $EpCAM^{-}$/ basal progenitor-enriched MCF10A mammary epithelial cells and CK5 and CK14 KD cells. Cultures were maintained for two weeks, after which they were fixed with PFA and stained with Dsg3 (green) and DAPI (blue). Representative immunofluorescence images of 3D mammospheroids are shown with magnifications from the indicated areas below (yellow boxes). Bar 100 μm. **B)** Immunofluoresence microscopy was used to detect cell-substrate adhesions from ctrl and CK5 KD cell lines. Specific antibody against focal adhesion marker vinculin (red) was used. Phalloidin was used to stain actin cytoskeleton (green) and DAPI (blue) for nuclei. Bar 20 μm. **C)** Traction force microscopy was applied to study cell-exerted forces of the ctrl, CK5- and CK14 KD cells doublets. Representative force maps from ctrl, CK5- and CK14 KD doublets after 3h incubation. **D)** Quantification of the Root Mean Square (RMS) tractions and Strain Energy (SE). Data are presented as box-plots. n(ctrl)=12, n(CK5 KD)=10 and n(CK14 KD)=10.

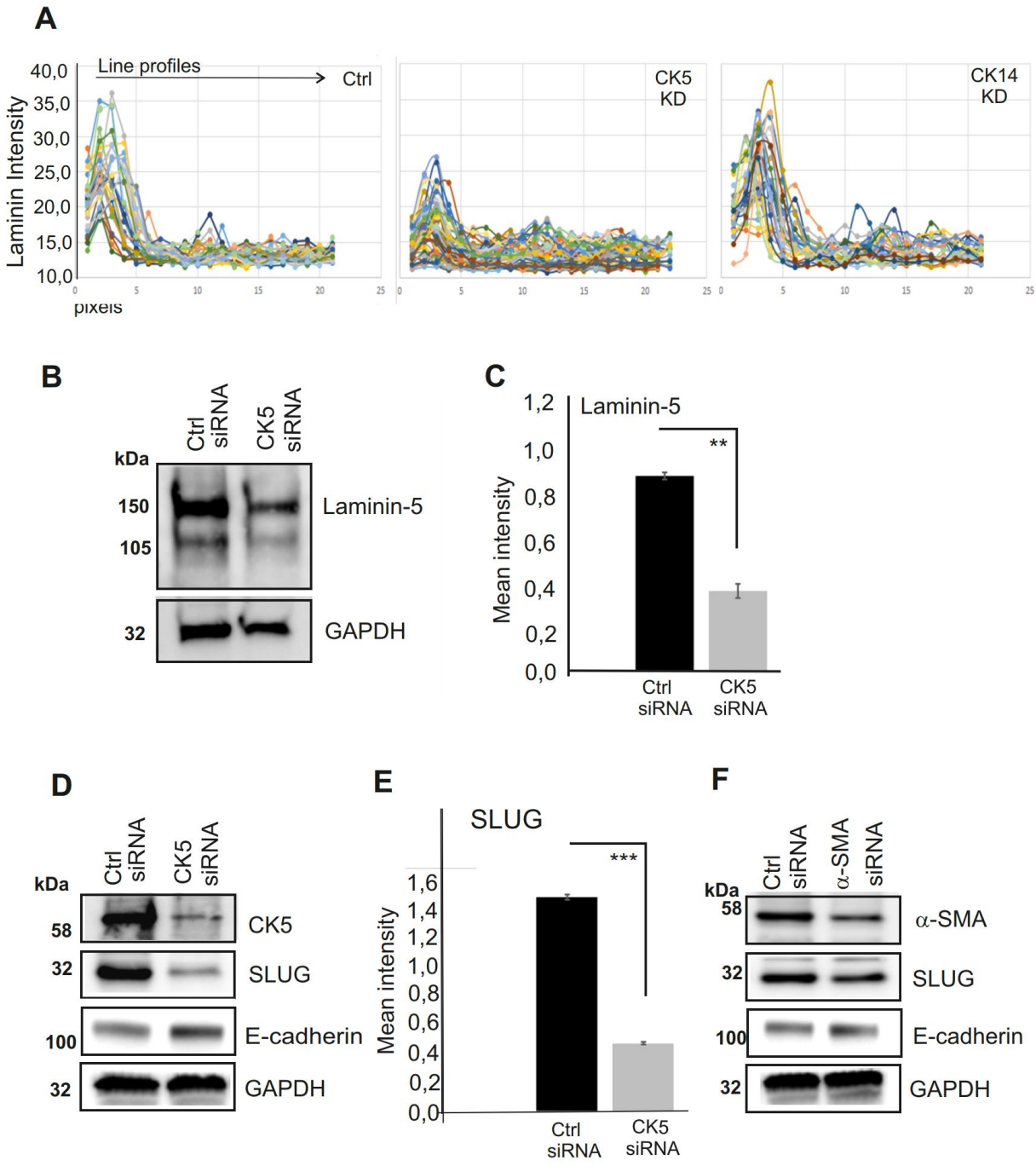


**Figure S8: Loss of CK5 impacts expression of laminin-5 and SLUG, Related to Figure 6. A)** CD49f$^{+}$ EpCAM$^{-}$/ basal progenitor-enriched MCF10A mammary epithelial cells, CK5 KD and CK14 KD cells were culture in 3D Matrigel for two weeks, after which they were fixed with PFA and stained with laminin-5 (See also Fig. 6A and B). Lineprofiles were drawn from the edge of the spheroid towards the center. 3-5 lineprofiles were drawn on each spheroid. Peak values on point 3 from lineprofiles were utilized for further analyses (Fig. 6B). **B)** Specific siRNAs against CK5 were

utilized in MCF10A cells. Cellular lysates were performed four days after incubation and specific antibody against laminin-5 was used in Western blotting. GAPDH was used as a loading control. Upper laminin-5 band (150 kDa) corresponds to the precursor form and lower band (105 kDa) to the mature form. **C)** Quantification of the mature laminin-5 levels from CK5-depleted cells, related to Figure S7B. Laminin-5 levels were divided with corresponding GAPDH values, and values of untreated samples were set to 1. Mean (± SEM) is shown; n=4; **P<0.01 (paired t-test). **D)** Specific siRNAs against CK5 were utilized in MCF10A cells. Cellular lysates were performed four days after incubation and specific antibodies against CK5, SLUG and E-cadherin were used in Western blotting. GAPDH was used as a loading control. **E)** Quantification of the SLUG levels from CK5-depleted cells, related to Figure S7D. SLUG levels were divided with corresponding GAPDH values, and values of untreated samples were set to 1. Mean (± SEM) is shown; n=3; ***P<0.001 (paired t-test). **F)** Depletion of α-SMA was performed with specific siRNAs in MCF10A cultures for four days. Cellular lysates from control siRNA and α-SMA siRNA treated cells were used in Western blotting and specific antibodies against α-SMA, SLUG and E-cadherin were utilized to assess their levels. GAPDH was used as a loading control.

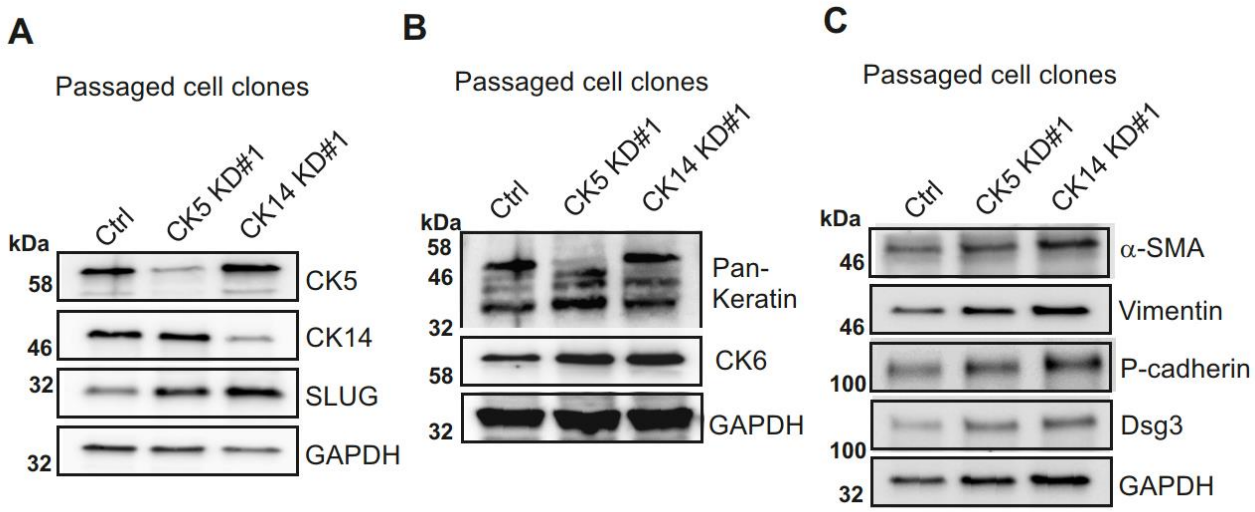


**Figure S9. Passaged CK5 and CK14 KD cell lines undergo compensation by other cytokeratins, Related to Figures 3-6. A)** Cellular lysates from passaged cell clones of ctrl ($CD49f^{+}$ $EpCAM^{-}$, enriched for basal progenitors), CK5 KD and CK14 KD cells were utilized in Western blotting. Specific antibodies against CK5, CK14 and SLUG were used to assess the levels of these proteins in clones that had been in culture for several weeks. GAPDH was used as a loading control. **B)** Cellular

lysates from passaged cell clones of ctrl ($CD49f^+$ $EpCAM^-$, enriched for basal progenitors), CK5 KD and CK14 KD cells were utilized in Western blotting and Pan-keratin and CK6 antibodies were used to detect possible compensation of the loss of CK5 and CK14. GAPDH was used as a loading control. **C)** Cellular lysates from passaged cell clones of ctrl ($CD49f^+$ $EpCAM^-$, enriched for basal progenitors), CK5 KD and CK14 KD cells were utilized in Western blotting. Antibodies against α-SMA, vimentin, P-cadherin and Dsg3 were used to assess the levels of these proteins in clones that had been in culture for several weeks. GAPDH was used as a loading control.

## REFERENCES


Cattavarayane, S., Palovuori, R., Ramanathan, J.T., and Manninen, A. (2015). α6β1- and αV-integrins are required for long-term self-renewal of murine embryonic stem cells in the absence of LIF. BMC Cell Biol. *16*, 3.

Chocteau, F., Abadie, J., Loussouarm, D., and Nguyen, F. (2019). Proposal for a histological staging system of mammary carcinomas in dogs and cats. Part 1: Canine mammary carcinomas. Front. Vet. Sci. *6*, 388.

Collins, L., Visscher, D., Simpson, J., and Schnitt, S.J. (2012). Usual ductal hyperplasia. In: Lakhani, S.R., Ellis, I.O., Schnitt, S.J., Tan, P.H., and van de Vijver, M. (eds.), World Health Organization Classification of Tumours: Pathology of the Breast, 4th ed., pp. 84-85. IARC, Lyon.

Ferreira, E., Gobbi, H., Saraiva, B.S., and Cassali, G.D. (2012). Histological and immunohistochemical identification of atypical ductal mammary hyperplasia as a preneoplastic marker in dogs. Vet. Pathol. *49*, 322-329.

Goldschmidt, M., Peña, L., Rasotto, R., and Zappulli, V. (2011). Classification and grading of canine mammary tumors. Vet. Pathol. *48*, 117-131.

Hutter, J. L., and Bechhoefer, J. (1993). Calibration of atomic-force microscope tips. Rev. Sci. Instrum. *64*, 1868-1873.

Krishnan, R., Park, C.Y., Lin, Y.-C., Mead, J., Jaspers, R.T., Trepat, X., Lenormand, G., Tambe, D., Smolensky, A.V., Knoll, A.H., et al. (2009). Reinforcement versus fluidization in cytoskeletal mechanoresponsiveness. PLoS ONE *4*, e5486.

LaBarge, M.A., Garbe, J.C., and Stampfer M.R. (2013). Processing of human reduction mammoplasty and mastectomy tissues for cell culture. J. Vis. Exp. *71*, e50011.

Mouser, P., Miller, M.A., Antuofermo, E., Badve, S.S., and Mohammed, S.I. (2010). Prevalence and classification of spontaneous mammary intraepithelial lesions in dogs without clinical mammary disease. Vet. Pathol. *47*, 275-284.

Ressel, L., Millanta, F., and Poli, A. (2011). Canine invasive lobular carcinoma of the mammary gland: Morphological and immunohistochemical characterizations of three cases. J. Comp. Path. *144*, 303-307.

Rønnov-Jessen, L., Petersen, O.W., and Bissell, M.J. (1996). Cellular changes involved in conversion of normal to malignant breast: Importance of the stromal reaction. Physiol. Rev. *76*, 69-125. Review.

Schnitt, S.J., Allred, C., Britton, P., Ellis, I.O., Lakhani, S.R., Morrow, M., Palazzo, J., Reynolds, C., Rutgers, E., Simpson, J., van de Vijver, M.J., and Vincent-Salomon, A. (2012b). Ductal carcinoma in situ. In: Lakhani, S.R., Ellis, I.O., Schnitt, S.J., Tan, P.H., and van de Vijver, M.J. (eds.), World Health Organization Classification of Tumours: Pathology of the Breast, 4th ed., pp. 90-94. IARC, Lyon.

Sneddon, I. N. (1965). The relation between load and penetration in the axisymmetric Boussinesq problem for a punch of arbitrary profile. Int. J. Eng. Sci. *3*, 47-57.

Simpson, J.F., Schnitt, S.J., Visscher, D., van de Vijver, M.J., and Ellis, I.O. (2012). Atypical ductal hyperplasia. In: Lakhani, S.R., Ellis, I.O., Schnitt, S.J., Tan, P.H., and van de Vijver, M.J. (eds.), World Health Organization Classification of Tumours: Pathology of the Breast, 4th ed., pp. 88-89. IARC, Lyon.

The Consensus Conference Committee (1997). Consensus conference on the classification of ductal carcinoma in situ. Cancer *80*, 1798-1802.

Tolić-Nørrelykke, I.M., Butler, J.P., Chen, J., and Wang, N. (2002). Spatial and temporal traction response in human airway smooth muscle cells. Am. J. Physiol. Cell Physiol. *283*, C1254-C1266.